Perimeter gating control and citywide dynamic user equilibrium: A macroscopic modeling framework

Deepak Ingole, Guilhem Mariotte, Ludovic Leclercq

Perimeter Gating Control and Citywide Dynamic User Equilibrium: a Macroscopic Modeling Framework

Deepak Ingole*, Guilhem Mariotte, Ludovic Leclercq

University of Lyon, IFSTTAR, ENTPE, 69120 Vaulx-en-Velin, France

Abstract

In recent years, several perimeter control strategies have been proposed for traffic management in cities. The common factor found in these works is the use of Macroscopic Fundamental Diagram (MFD) models to describe the dynamics of the network and optimize traffic inside the perimeter by manipulating perimeter inflows. Perimeter gating control strategies are attractive for traffic management inside the inner city. However, it inevitably creates a negative impact on the traffic outside. Most of the works in this research area have neglected vehicle rerouting outside the controlled perimeter, i.e., they do not consider demand elasticity to the central region resulting from gating and the related queues. In this paper, we propose a global modeling framework capable of assessing the effect of perimeter gating control (in terms of queue, emission, and total time spent) on the full network, considering demand elasticity resulting from Dynamic User Equilibrium (DUE). Classical Proportional-Integral (PI) control scheme is used to control traffic congestion inside a central region (reservoir). The modeling framework is comprised of: (i) an accumulation-based MFD model to reproduce traffic dynamics inside the reservoir, (ii) point-queue model to represent queuing vehicles on inbound links to the gating points, and (iii) a time-dependent travel time profile based on a steady-state approximation of MFD dynamics to characterize the alternative road network (bypass). DUE is then implemented,

*Corresponding author
Email addresses: deepak.ingole@ifsttar.fr (Deepak Ingole), guilhem.mariotte@ifsttar.fr (Guilhem Mariotte), ludovic.leclercq@ifsttar.fr (Ludovic Leclercq)

considering instantaneous predicted travel time. This determines how the demand to the inner region is affected by the gating. The functioning of the global system is assessed by total time spent and NOx and CO_2 emissions inside the reservoir and for the full network. The presented simulation results show that the perimeter gating control helps to maintain congestion at the desired level with significant improvements in the total time spent and the mean speed in the network. However, it shows a slight increase in the queues. As expected, deviation to the bypass alternative is significant and should not be neglected when carrying out a global assessment of gating system performance.

Keywords: Traffic dynamics, MFD, routing, travel time estimation, perimeter gating control, emission.

---

1. Introduction

Nowadays, traffic congestion is a crucial issue in metropolitan cities. Traffic congestion not only causes traffic delays but also increases fuel consumption and results in health issues for the inhabitants. Researchers and engineers are developing new strategies and infrastructures to deal with traffic congestion. Over the last two decades, the application of control systems engineering to traffic congestion has gained significant attention by ensuring the efficient and reliable operation of urban traffic networks (for a review refer to Papageorgiou et al. (2003); Wang (2010); Zhao et al. (2012); Zhong et al. (2018a)). In recent years, significant efforts have been made to provide efficient solutions to urban traffic problems. These efforts have mainly been directed in two directions: first, the modeling of urban networks; second, their control.

Regarding urban network modeling, the concept of Macroscopic Fundamental Diagram (MFD) has been used since the 1970s. This concept provides for network regions a well-defined relation between space-mean flow and density (or vehicle accumulation). The idea behind the MFD was initially proposed by Godfrey (1969) and similar approaches were introduced later by Mahmassani et al. (1984); Daganzo (2007). It was first tested in a field experiment in

the city of Yokohama, Japan and revealed that the MFD exists over a large urban area (Geroliminis and Daganzo, 2008).

In the literature, there are two forms of MFD models: accumulation-based and trip-based models. The accumulation-based model is simply a conservation equation where the outflow is determined by the MFD function. This model has been criticized recently (see Mariotte and Leclercq (2018); Lamotte et al. (2018)) because outflow overreacts to sudden inflow surges, leading to incorrect travel time situations. The trip-based model has been proposed (Mariotte et al., 2017) to circumvent this issue. It tracks vehicle traveled distance inside the reservoir while assigning the same instantaneous speed to all vehicles defined by the MFD. The most recent studies (Mariotte and Leclercq, 2018; Leclercq and Paipuri, 2018; Mariotte and Leclercq, 2019) have shown that the trip-based model provides significant improvements in free-flow but that the accumulation-based model certainly appears better during saturation and congestion periods. These periods are predominant when traffic conditions are critical. Thus, the accumulation-based MFD model is used in this paper.

The issue of traffic congestion in large urban networks can be solved using perimeter control (i.e., manipulating the traffic flow at the periphery of a city or its central business district). In recent years, different classical and advanced control strategies have been implemented for traffic control, considering the city as a single reservoir or partitioned into multiple reservoirs. The classical Proportional-Integral (PI) controller was designed for the control of an urban network in China and in Greece (Keyvan Ekbatani et al., 2016). The multi-variable feedback regulator considering three reservoirs was designed for the traffic network of San Francisco (Aboudolas and Geroliminis, 2013). Both controllers were constructed for reference tracking purposes using a linearized model of the network. The reference trajectory was chosen in such a way that the value varies in the uncongested regime of the MFD having a positive slope and close to the critical value of the controlled variable. Moreover, in both works, the constraints on the input variable were imposed after controller action was obtained. The advantage of these controllers is that they are computationally

efficient and easy to design, but the downside is that they do not consider the constraints explicitly as a part of the controller. To overcome the downside of the works mentioned previously, the robust PI controller (based on Quantitative Feedback Control (QFT) theory) for the uncertainty linear model of an urban region was presented in Haddad and Shraiber (2014). The robust controller was also designed to handle the control constraints within the design level in a systematic way, where the constraints are explicitly integrated utilizing the so-called describing function. The solution of the control problem in a bi-model multi-region urban network is presented in Ampountolas et al. (2017) with a robust PI controller. The reference model adaptive control approach was implemented to design distributed adaptive perimeter control laws Haddad and Zheng (2018); Haddad and Mirkin (2017). Recently, perimeter flow control with an observer-based H_∞ Proportional (P) and Proportional-Integral (PI) controllers based on Lyapunov theory were presented in Mohajerpoor et al. (2019).

With respect to advanced control strategies, Model Predictive Control (MPC) has been employed for the perimeter control of single and multi-region cities, considering non-linear, linear, and hybrid models of an urban network. To solve the perimeter control problem several MPC approaches have been used, such as linear MPC (Kouvelas et al., 2017b), non-linear MPC (Geroliminis et al., 2013), hybrid MPC (Lin et al., 2011), distributed MPC (Majid et al., 2014), economic MPC (Sirmatel and Geroliminis, 2017), robust MPC (Tettamanti et al., 2014), two-level hierarchical MPC (Zhou et al., 2017), *etc.* The MPC schemes mentioned above can be designed for different objectives, such as state regulation, output tracking, profit maximization *etc.* However, the success of MPC is mainly dependent on the accuracy of the prediction model (Maciejowski, 2002). It is well-known that different types of uncertainty can be integrated in the MFD model of heterogeneous networks (Daganzo et al., 2011) or model parameters. To deal with uncertainty in MFD models, a robust perimeter control scheme has been designed using different approaches, such as Linear Matrix Inequalities (LMI) optimization (Ampountolas et al., 2014), interpolation (Haddad, 2015), control-lyapunov function (Zhong et al., 2018a), Sliding Mode Control

(SMC) (Aalipour et al., 2018), *etc.* In Haddad (2017) the optimal control policy to maximize the total network throughput was designed for the perimeter control of two urban regions.

Due to the limitations of model-based control strategies, the authors in Li et al. (2012) introduced a concept of fixed-time signal timing perimeter control. A generic real-time feedback-based gating concept was proposed for perimeter control (see Keyvan-Ekbatani et al. (2012, 2014)). Not all these perimeter control works explore the actuation of vehicle routing outside the perimeter in detail. The authors in Hajiahmadi et al. (2013) and Yildirimoglu et al. (2015) used optimal dynamic traffic route guidance to solve the problem of congestion in multiple MFD sub-regions. To control the perimeter flow rate, the work in Sirmatel and Geroliminis (2017) and Ding et al. (2017) coupled optimal traffic guidance with boundary control and proposed an optimization method aimed at minimizing total network delay. This approach provides a solution to traffic congestion but does not consider the influence of the control method on network state transition, which may cause hysteresis in the network or local gridlock in the optimal regulation rate of excessive flows. Recently, learning-based approach have been used in perimeter control, e.g., reinforcement learning (Ni and Cassidy, 2019). These works deal with optimal route guidance without considering user compliance with instructions. Nor do they consider current behaviors of user who try to optimize their trip in a selfish way by finding their shortest-path, referred to as user equilibrium in the literature. To deal with the waiting queues at the perimeter, authors in Hajiahmadi et al. (2015); Keyvan-Ekbatani et al. (2016); Kouvelas et al. (2017a) has derived an optimal perimeter control policy that explicitly considered the effect of queuing vehicles on traffic flow dynamics but not the elasticity of demand for the inner regime, i.e., users who take an alternative path due to the queues to enter the perimeter. In Kim et al. (2018) investigated the influences of boundary capacity, outflow restriction, and demand ratio on traffic dynamics. The perimeter control of a mixed-network consisting of a freeway and urban region was designed using MPC (see Haddad et al. (2013); Frejo et al. (2014)).

This literature review shows that vehicle routing strategies outside the perimeter is a blind spot regarding perimeter control works based on MFD. Deriving a modeling framework to account for this specific problem is not trivial. In particular, multi-reservoir systems that are a direct extension of the MFD model in the inner-region are not ideal because all the surrounding reservoirs are defined by a single speed whatever the number of vehicles that want to enter the reservoir or bypass it. Thus, locally there is no gain in switching to another alternative despite the fact that in reality there are queues due to gating. Therefore, we need to design a new modeling framework to properly isolate the queues entering the controlled area and clearly differentiate other alternatives.

In this paper, we present a perimeter gating control scheme to control traffic congestion in an urban network with three regional routes (one "internal" route representing internal trips and two "transfer" routes representing trips with different lengths crossing the reservoir). We call it gating and not perimeter control, as the different entries are monitored separately and exit flows are not controlled. One of these routes has an external alternative for routing, corresponding to the roads that permit bypassing the inner reservoir. A classical PI control scheme is applied to control total accumulation inside the perimeter by manipulating traffic inflow through the gates at the entry of two transfer routes.

Generally in perimeter control, congestion from inside the reservoir is moved to the outside by manipulating the inflows that create queues outside the perimeter. In our settings, we consider that for one Origin-Destination (OD) pair a bypass option exists in addition to the route that enters the reservoir. The total input demand for this OD pair is distributed along the transfer and bypass road options by solving the Dynamic User Equilibrium (DUE) problem. By doing so, we consider user adaption to the perimeter control. This requires designing a new modeling framework to handle flows and queues on the different itineraries outside the reservoir. The main contribution of this paper compared to previous works is that the external UE discipline makes the input demand elastic from the standpoint of the reservoir. The evaluation of global system performance

is therefore much more realistic. Note that the way we implement external UE discipline in the MFD framework also represents another contribution as we formulate the DUE of predicted travel times without re-routing using usual quasi-static approximation.

The rest of paper is organized as follows. The urban network under consideration is introduced in the next section. Section 2 sets out the problem statement of this work. In Section 3, an overview of the global modeling framework along with the routing scheme and emission laws is given. Section 4 provides a description of the design of the perimeter gating control scheme. Section 5 gives the results of presented approach while the concluding remarks are given in Section 6.

2. Problem Statement

The network under consideration corresponds to a homogeneous urban reservoir with one internal regional route, two external regional routes that cross the reservoir, and one bypass option as depicted in Fig. 1. In this work, a regional route, or simply "route" in the following, corresponds to the aggregation of multiple individual paths in the real city street network which share characteristics in common (*e.g.*, similar topology or length, following the same sequence of reservoirs in multi-reservoir systems, *etc*). Both external routes also include an Inbound Link (IL) at the reservoir entry. This represents the aggregation of all portions of the road on which vehicles may wait due to inflow limitation (natural propagation of congestion or action of the controllers).

We assume that the traffic dynamics of the reservoir is described by a well-defined production-MFD $P(n)$ (in [veh·m/s]), or equivalently, a speed-MFD $V(n)$ (in [m/s]), where n (in [veh]) is the total number of vehicles circulating in the reservoir. Production-MFD is defined by the following characteristic values: jam accumulation n_j, critical accumulation n_c, maximum production or capacity $P_c = P(n_c)$, and free-flow speed $\tilde{v} = dP(0)/dn$. We consider the accumulation-based model presented in Yildirimoglu and Geroliminis (2014)

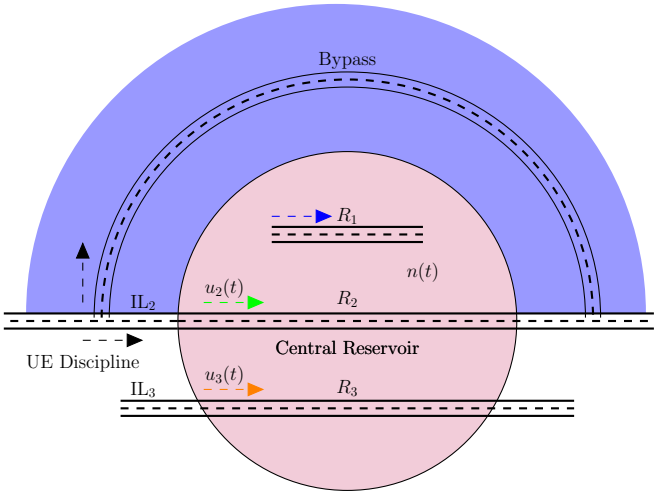

Fig. 1: Two bin network with one central reservoir and bypass option: one internal route (R_1), two external routes (R_2 & R_3), two perimeter control inputs $u_2(t)$ and $u_3(t)$, and one measured output $n(t)$ as total accumulation inside the reservoir.

and further extended in Mariotte and Leclercq (2018). It considers different trip lengths inside the reservoir, the proper treatment of the input and output flow of the reservoir based on the constraints on flow and travel production, and accounts for the effect of internal trips.

The objective of this work is to investigate the impact of the gating control on routing inside-and-outside the reservoir and see how the controller reacts to the routing scheme. Gating control is applied to track desired accumulation ($n(t)$) inside the reservoir by manipulating two input flows ($u_2(t)$ and $u_3(t)$) at the perimeter. We design two PI controllers with the anti-windup scheme and saturation limits on manipulated variables; routing discipline is designed based on UE obtained by exact predictive travel time. Different scenarios will be considered for this network to cover the most usual congestion situations (resulting from internal flow or from downstream spillbacks on routes 2 or 3).

3. Traffic Modeling

In this section, we introduce the dynamics of both the accumulation-based MFD model of the central reservoir and the simplified model of the peripheral reservoir where users can re-route. The total system includes three regional routes inside the central reservoir and a bypass route inside the peripheral reservoir.

3.1. Central reservoir dynamics

First, we focus on traffic dynamics inside the central reservoir. The accumulation-based model with $\mathcal{N}$ regional routes of lengths L_i has been fully described in Mariotte and Leclercq (2018, 2019). The accumulations n_i are the numbers of vehicles traveling on each route i inside the reservoir, satisfying the following system (Geroliminis, 2015):

$$\frac{dn_i}{dt} = q_{\text{in},i}(t) - q_{\text{out},i}(t), \qquad \forall i \in \{1, \dots, \mathcal{N}\}, \tag{1}$$

where $q_{\text{in},i}(t)$ and $q_{\text{out},i}(t)$ are respectively the effective inflow and outflow for route i.

In this work, we use the model of flow exchange at the perimeter proposed by Mariotte and Leclercq (2018, 2019) to define $q_{\text{in},i}(t)$ and $q_{\text{out},i}(t)$. The effective inflow $q_{\text{in},i}(t)$ for a transfer route i is the result of the competition between a corresponding demand $\lambda_i(t)$, an entry supply function $I_i(n_i, n)$, and control actions at gates $u_i(t)$. We also account for a queue at the entry of each route (described by a point-queue model) to store the waiting vehicles when the demand is not satisfied. These vehicles are physically waiting on the corresponding inbound link in our network. The inflow of an internal route is assumed to be unrestricted, thus equal to its demand:

$$q_{\text{in},i}(t) = \begin{cases} \min(\lambda_i(t - \tilde{T}_{IL,i}), I_i(n_i(t), n(t)), u_i(t)), & \text{for a transfer route,} \\ \lambda_i(t), & \text{for an internal route,} \end{cases} \tag{2}$$

where $u_i(t)$ is the gating inflow obtained by PI controller. The inflow demand for any transfer route i is shifted from $\tilde{T}_{IL,i}$, which corresponds to the free-flow

travel time required to transfer through the inbound link before reaching the reservoir entry. We have $\tilde{T}_{IL,i} = L_{IL,i}/\tilde{v}_{IL,i}$, where $L_{IL,i}$ is the length of the inbound link i and $\tilde{v}_{IL,i}$ its free-flow speed. The entry supply function is given by

$$I_i(n_i, n) = \begin{cases} \frac{n_i}{n}\frac{\alpha P_c}{L_i}, & \text{if } n < n_c, \\ \frac{n_i}{n}\frac{\alpha P(n)}{L_i}, & \text{otherwise.} \end{cases} \tag{3}$$

We decided to adopt a shape similar to that of Mariotte and Leclercq (2018, 2019), who discussed the role of the entry supply function. The purpose of coefficient $\alpha > 1$ is to let the total inflow temporarily exceed the reservoir capacity. In this work, we have chosen $\alpha = 1.3$ quite empirically, as shown in Fig. 2.

In case of an inflow limitation due to either the control gating or the entry supply function, the accumulation in each inbound link (IL, i) stores the vehicles queuing to enter the reservoir. It is governed by the following conservation equation

$$\frac{dn_{IL,i}}{dt} = q_{\text{in},IL,i}(t) - q_{\text{out},IL,i}(t), \tag{4}$$

where the inflow of the IL i is equal to the route demand $q_{\text{in},IL,i}(t) = \lambda_i(t)$, and its outflow to the inflow on route i, i.e., $q_{\text{out},IL,i}(t) = q_{\text{in},i}(t)$. For route 2, the inbound link inflow is modified when users prefer switching to the bypass route according to the UE principle. This is detailed further in subsection 3.3.

Because they are the result of the reservoir inner dynamics, the outflows $q_{\text{out},i}(t)$ are all inter-dependent through the following relationships between the most constrained outflow k and other effective outflows i written as:

$$q_{\text{out},k}(t) = \min(\mu_k(t), O_k(n_k, n)), \tag{5}$$

where $k = \arg\min_{1 \le i \le N} \frac{\mu_i}{O_i(n_i,n)}$ and

$$q_{\text{out},i}(t) = \frac{n_i(t)}{n_k(t)}\frac{L_k}{L_i} q_{\text{out},k}(t), \qquad \forall i \neq k. \tag{6}$$

Function $O_i(n_i, n)$ is the demand for outflow of route i. As in (Mariotte and Leclercq, 2018, 2019), in over-saturated situations, we assume this demand to

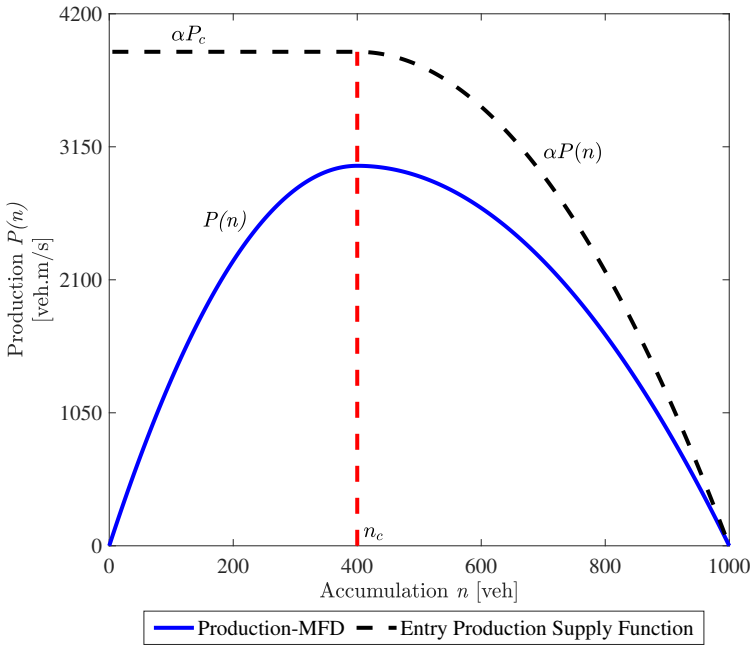

Fig. 2: Production-MFD and production entry supply function.

be maximum for transfer routes (outflow at the reservoir exit border), and to decrease along the production-MFD for internal routes (the rate at which destinations are reached inside the reservoir):

For a transfer route:

$$O_i(n_i, n) = \begin{cases} \frac{n_i}{n}\frac{P(n)}{L_i}, & \text{if } n < n_c, \\ \frac{n_i}{n}\frac{P_c}{L_i}, & \text{otherwise.} \end{cases} \tag{7a}$$

For an internal route:

$$O_i(n_i, n) = \frac{n_i}{n}\frac{P(n)}{L_i}. \tag{7b}$$

For more details on the considered accumulation-based model see Mariotte et al. (2017); Mariotte and Leclercq (2018, 2019).

3.2. Bypass Road Network

The bypass road network is considered as a second single reservoir but with simplified traffic dynamics. The reason for doing this is that it is very challeng-

ing and often uncertain to seek instantaneous dynamic equilibrium between two alternatives with fast varying travel time functions. Whereas the travel time dynamics of traffic entering the city reservoir must be monitored closely due to the considerable influence of gating, the alternative road network can be characterized by a piecewise constant travel time. The idea is that this alternative option corresponds to the bypass around the city center, which is subject to slow-varying traffic conditions as it is located in a much less dense urban area. Therefore, we can reproduce the evolution of travel time in the reservoir representing the alternative, by using the steady-state approximation of the MFD dynamics. In practice the mean speed for the next time period is derived from the MFD speed function, considering the current accumulation at the beginning of the time period.

Therefore, in comparison with the city center represented by the central reservoir which is that most likely to undergo highly dynamic traffic conditions, the assumption of a piecewise constant travel time evolution in the peripheral reservoir seems reasonable. In order to track the slow variations of traffic conditions in the latter, we define its speed-MFD function as follows:

$$v_p(n_p) = \tilde{v}_p(1 - n_p/n_{j,p})^2, \tag{8}$$

where v_p is the mean speed function depending on its current accumulation n_p, $\tilde{v}_p$ is its free-flow speed and $n_{j,p}$ its jam accumulation. The actual mean speed v_p^m of the reservoir is considered constant for a fixed period of Δt_p, from $t = m\Delta t_p$ to $t = (m+1)\Delta t_p$, after which it is updated according to the new accumulation value $n_p(t)$ at $t = (m+1)\Delta t_p$. The actual travel time for users entering this reservoir at $t = m\Delta t_p$ is approximated as $T_p^m = L_p/v_p^m$. Then, the bypass reservoir dynamics are described by the following conservation equation with a fixed delay (the constant travel time T_p^m)

$$\frac{dn_p}{dt} = q_{\text{in},p}(t) - q_{\text{in},p}(t - T_p^m). \tag{9}$$

The inflow into this bypass route is defined after UE discipline for users entering inbound link 2, as detailed in the following subsection.

3.3. User Equilibrium discipline

As shown in Fig. 1, the users willing to enter route R_2 can choose to take the bypass route instead of entering the inbound link and crossing the reservoir to reach their destination. Let us first assume that we have $m\Delta t_p < t < (m+1)\Delta t_p$. If we assume that these travelers are making their choices according to DUE, we should have the following relationships in travel time at t:

$$\begin{cases} T_{IL,2}(t) + T_2(t + T_{IL,2}(t)) < T_p^m & \Leftrightarrow \text{no one chooses the bypass,} \\ T_{IL,2}(t) + T_2(t + T_{IL,2}(t)) = T_p^m & \Leftrightarrow \text{at least one user chooses the bypass,} \end{cases} \tag{10}$$

where T_p^m is the travel time of the bypass route, $T_{IL,2}(t)$ and $T_2(t)$ are the exact predictive travel times on the inbound link and in the central reservoir, respectively, for route R_2 (that will be experienced by users entering the reservoir or the inbound link at t). The inbound link is assumed to consist of two parts: the first one is free-flow with travel time $\tilde{T}_{IL,2}$, and the second one is congested, dynamically represented by a point-queue model. Thus, its travel time consists of two terms: $T_{IL,2}(t) = \tilde{T}_{IL,2} + \delta_{IL,2}(t + \tilde{T}_{IL,2})$, where $\delta_{IL,2}(t)$ is the exact predictive delay in the inbound link (that will be experienced by users willing to enter the reservoir at t). Both $\delta_{IL,2}(t)$ and $T_2(t)$ are the result of traffic dynamics that will be observed inside the reservoir after t. During the simulation, we cannot estimate this delay and travel time at t without knowing the future evolution of the reservoir. Consequently, we have implemented a two-step simulation process that first permits obtaining the predictive travel time in the direction of the reservoir and, second, determines the path flow distribution over the routes based on DUE.

Step 1 Perform first simulation without the bypass route (T_p^m is set to infinity) and calculate $T_{IL,2}(t)$ and $T_2(t)$.

Step 2 Perform second simulation with the bypass route and divert users to it once the condition $T_{IL,2}(t) + T_2(t + T_{IL,2}(t)) = T_p^m$ is satisfied (the travel

times are known from the previous simulation). Once users are diverted to the bypass route, the inbound link delay will be changed. The new evolution of this delay is determined by the UE condition $T_{IL,2}(t)+T_2(t+T_{IL,2}(t)) = T_p^m$.

As presented in Fig. 3, the exact predictive delay and travel time are calculated based on the cumulative entering curves $N_{\text{in},IL,2}(t)$, $N_{\text{in},2}(t)$, and exiting curves $N_{\text{out},2}(t)$, which are direct outputs from the single reservoir simulation (integration of the effective flows over the simulation period). Switching the users to the bypass is achieved by splitting the inflow demand $\lambda_2(t)$ into the inbound link inflow $q_{\text{in},IL,2}(t)$ and the bypass route inflow $q_{\text{in},p}(t)$ according to the following scheme:

$$\begin{cases} \left.\begin{aligned} q_{\text{in},IL,2}(t) &= \lambda_2(t), \\ q_{\text{in},p}(t) &= 0, \end{aligned}\right\} & \text{if } T_{IL,2}(t) + T_2(t') < T_p^m, \\ \left.\begin{aligned} q_{\text{in},IL,2}(t) &= q_{\text{out},2}(t''), \\ q_{\text{in},p}(t) &= \lambda_2(t) - q_{\text{in},IL,2}(t), \end{aligned}\right\} & \text{if } T_{IL,2}(t) + T_2(t') = T_p^m, \end{cases} \tag{11}$$

where $t' = t + T_{IL,2}(t)$ and $t'' = t' + T_2(t')$ (see also Fig. 3). By setting the inbound link inflow to $q_{\text{out},2}(t'')$ once $T_{IL,2}(t)+T_2(t') = T_p^m$, we ensure that the latter equality (the DUE condition) is always satisfied as long as some users are diverted to the bypass.

When an update in the bypass route travel time T_p^m occurs, the previous scheme must be adjusted to ensure the proper transition between T_p^m and T_p^{m+1}. Two cases are distinguished, as presented in Fig. 4. The first one is when $T_p^m < T_p^{m+1}$, which means that the peripheral reservoir is being loaded, resulting in a decrease in its mean speed. In this case, fewer users will switch to the bypass route, so that the inbound link of route 2 is temporarily loaded at a maximum rate of $q_{\max}$ during a period of Δt. The exact duration of this transient period is calculated to adjust UE conditions to the new value of T_p^{m+1}, as illustrated in Fig. 4(a). Thus, we have, after the update of T_p^m, for $(m+1)\Delta t_p < t < (m+1)\Delta t_p + \Delta t$, and if $T_{IL,2}(t) + T_2(t + T_{IL,2}(t)) \geq T_p^{m+1}$ (users are still

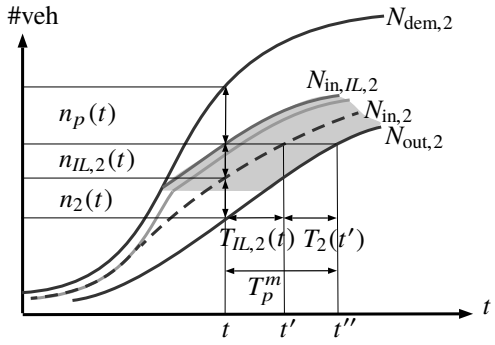

Fig. 3: Cumulative count curves for route R_2 and the bypass route (demand curve, entering curve to the inbound link, entering and exiting curves of route R_2 in the reservoir). Exact predictive travel times and accumulations are mentioned for a given time t. The gray line splits the inbound link into free-flow and congested parts (delay). The gray area indicates when $T_{IL,2}(t) + T_2(t') = T_p^m$.

switching to the bypass route):

$$\begin{cases} q_{\text{in},IL,2}(t) = \min\left(q_{\max}, \lambda_2(t)\right), \\ q_{\text{in},p}(t) = \lambda_2(t) - q_{\text{in},IL,2}(t), \end{cases} \tag{12}$$

$$\Delta t = \frac{q_{\text{out},2}(t')(T_p^{m+1} - T_p^m)}{q_{\max} - q_{\text{out},2}(t')} \tag{13}$$

where $t' = t + T_p^m$. The calculation of Δt is deduced from the expression of the number of vehicles impacted ΔN, calculated as $\Delta N = q_{\max}\Delta t$ and $\Delta N = q_{\text{out},2}(t')\Delta t + q_{\text{out},2}(t')(T_p^{m+1} - T_p^m)$.

The second case is when $T_p^m > T_p^{m+1}$, which means that the peripheral reservoir is released so that its mean speed increases. In this case, more users can eventually switch to the bypass route, so that the inbound link 2 is temporarily loaded at a minimum rate of $q_{\min}$ during Δt. As previously, the duration of the transient period is calculated in compliance with UE conditions, as shown in Fig. 4(b). Thus, after the update of T_p^m, we have $(m+1)\Delta t_p < t < (m+$

1)$\Delta t_p + \Delta t$, and $T_{IL,2}(t) + T_2(t + T_{IL,2}(t)) \geq T_p^{m+1}$:

$$\begin{cases} q_{\text{in},IL,2}(t) = \min\left(q_{\min}, \lambda_2(t)\right), \\ q_{\text{in},p}(t) = \lambda_2(t) - q_{\text{in},IL,2}(t), \end{cases} \tag{14}$$

$$\Delta t = \frac{q_{\text{out},2}(t')(T_p^m - T_p^{m+1})}{q_{\text{out},2}(t') - q_{\min}}, \tag{15}$$

where $t' = t + T_p^m$. These maximum and minimum flows $q_{\max}$ and $q_{\min}$ applied to the inbound link are set in our modeling only to avoid instantaneous switching between the latter and the bypass route.

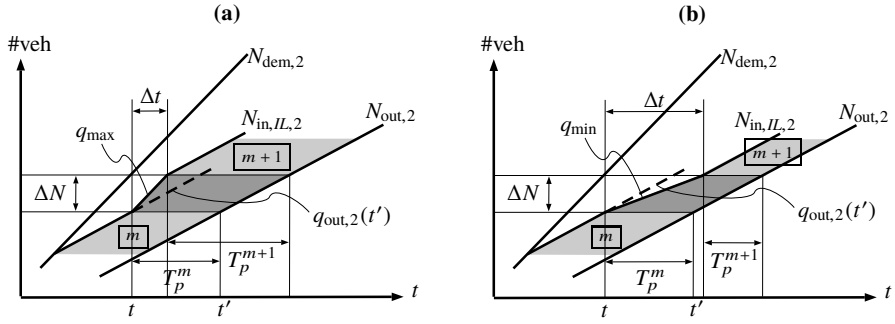

Fig. 4: Detail of the cumulative count curves for route R_2 and the bypass route that illustrate changes in the bypass route travel time. (a) Case when $T_p^m < T_p^{m+1}$, and (b) when $T_p^m > T_p^{m+1}$.

3.4. Emission Laws

Emission laws are required to calculate total emission when performing the overall assessment of the urban network. Here, we use macroscopic relationships that provide the emission rate (in [g/km]) of a vehicle fleet depending on the mean speed $v^*(t)$. These rules are taken from the COPERT IV framework (Ntziachristos et al., 2009) and have been integrated with the fourth-degree polynomial for simplicity Lejri et al. (2018).

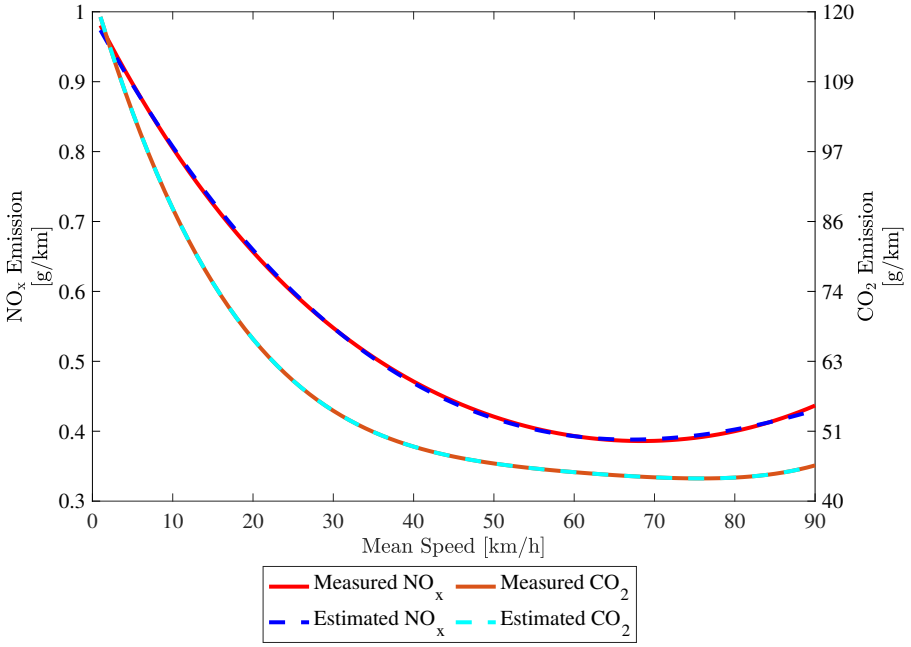

Fig. 5: Measured and estimated emission factor of NO_x and CO_2 for varying mean speed.

Fig. 5 shows the emission levels of NO_x and CO_2 for different mean speeds of the vehicle. The emission model for NO_x is given as

$$EF_{\mathrm{NOx}}(v) = p_1 v^3 + p_2 v^2 + p_3 v + p_4, \tag{16}$$

where the values of coefficients p_1, p_2, p_3, and p_4 are -6.142×10^{-7}, 2×10^{-4}, -2.08×10^{-2}, and 9.944×10^{-1}, respectively. The emission model for CO_2 is given as

$$EF_{\mathrm{CO_2}}(v) = p_1 v^4 + p_2 v^3 + p_3 v^2 + p_4 v + p_5, \tag{17}$$

where the values of coefficients p_1, p_2, p_3, p_4, and $p_5$are 4.1526×10^{-6}, -1.0412×10^{-3}, 1.0017×10^{-1}, -4.4723, and 123.5378, respectively.

In this work, we obtained the Emission Factor (EF) model of Nitrogen Oxide (NOx) and Carbon Dioxide (CO_2) based on the measured emission data with the mean speed (v^*) profile of private cars. Then, the evolution of emission level

$E_{dt}(t)$ (in [g]) of one pollutant between t and $t + dt$ is calculated as:

$$E_{dt}(t) = EF(v^*(t)) \times n^*(t) \times v^*(t) \times dt, \tag{18}$$

where $EF(v^*(t))$ is the emission factor of the pollutant considered (in [g/km]), $n^*(t)$ the accumulation and $v^*(t)$ the mean speed at t. The value of $EF(v^*)$ is estimated by (16) and (17). $E_{dt}(t)$ corresponds to instantaneous emissions, as it is calculated for a small time step $dt = 1$ s. On route i in the reservoir, $n^*(t)$ is the partial accumulation $n_i(t)$, and $v^*(t)$ is the central reservoir mean speed $v(t)$. In the IL for route i, $n^*(t)$ is the link accumulation $n_{IL,i}(t)$, and $v^*(t)$ is the link mean speed $v_{IL,i}(t)$. On the bypass route, $n^*(t)$ is the peripheral reservoir accumulation $n_p(t)$, and $v^*(t)$ is its current mean speed v_p^m. The mean speed in inbound link i is obtained as:

$$v_{IL,i}(t) = \frac{L_{IL,i}}{T_{IL,i}(t)}, \tag{19}$$

where $L_{IL,i}$ and $T_{IL,i}$ are respectively the inbound link length and travel time.

4. Gating Control Strategy

The Proportion-Integral (PI) controller has been the most popular and the most commonly used industrial controller in recent years. In the traffic control literature it has been shown that gain-based control algorithms such as PI and Proportion-Integral-Derivative (PID) controllers provide cost-effective and pragmatic solutions for handling uncertainties and bounded disturbance effects (see Keyvan Ekbatani et al. (2016); Aboudolas and Geroliminis (2013); Haddad and Shraiber (2014); Ampountolas et al. (2017); Haddad and Mirkin (2017); Zhong et al. (2018a,b)). As mentioned in the introduction, our objective is to investigate the impacts of perimeter control and therefore we used a well-known and classical PI controller.

The application of a PI controller in a perimeter control scheme is shown in Fig. 6, where r is the desired reference (total accumulation inside the reservoir, $n_c(t)$), y is the output of the reservoir (measured total accumulation in the

reservoir, $n(t)$) obtained by the traffic dynamics as in (1), e is the error between the reference and output, and u is the vector of control actions (gating flow, $u_i(t)$). The PI controller manipulates the traffic flow rate of the route 2 ($u_2(t)$) and route 3 ($u_3(t)$) while the flow rate to the internal trip route 1 ($u_1(t)$) is kept constant.

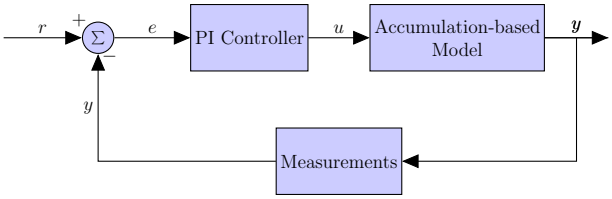

Fig. 6: A block diagram of closed-loop perimeter gating control using the PI controller.

The simplest form of the PI controller in continuous-time is given by

$$u(t) = k_P e(t) + k_I \int_0^t e(\tau) d\tau, \tag{20}$$

where u is the control input, e is the error between the reference and the output, and k_P and k_I are the proportional and integral gain, respectively. The proportional action is related to the typical operation of increasing the control variable when the control error is large (with the appropriate sign) and integral action is related to the past values of the control error. The discrete time equivalent expression is:

$$u(k) = k_P e(k) + k_I T_s \sum_{j=0}^{k} e(j), \tag{21}$$

where T_s is the sampling time of the system. In this work, we applied the clamping anti-windup scheme with saturation limits on the inputs to avoid the integrator windup phenomenon (Visioli, 2006, Chapter 3). The desired reference value ($n_c(t)$) is set to the critical density inside the reservoir, as this guarantees maximized outflow.

5. Simulation Results

In this section, we present the simulation results of the gating control scheme with DUE discipline applied to the network considered, as shown in Fig. 1. We

consider three case studies where congestion is created by increasing internal trips or by imposing flow restrictions on the output of routes 2 and 3. The global parameters used for all the case studies are listed in Table 1.

Table 1: Values of the parameters used in the case study.

Component	**Parameter**	**Value**	**Unit**
Central reservoir	trip lengths (L_i)	[1600 2000 1500]	m
	maximum production (P_c)	3000	veh.m/s
	free-flow speed ($\tilde{v}$)	15	m/s
	jam accumulation (n_j)	1000	veh
	critical accumulation (n_c)	400	veh
Peripheral reservoir	trip length (L_p)	22500	m
	free-flow speed ($\tilde{v}_p$)	25	m/s
	free-flow travel time ($\tilde{T}_p$)	900	s
	jam accumulation ($n_{j,p}$)	8100	veh
	update period (Δt_p)	600	s
Inbound links	free-flow speed ($\tilde{v}_{IL,i}$)	[0 25 25]	m/s
	trip length ($L_{IL,i}$)	[0 2500 2500]	m

In each case, user equilibrium is derived from instantaneous exact predictive travel time in the reservoir. Apart from the main objective of the controller to track the desired reference, we investigate several other parameters, such as the Total Time Spent (TTS) in the network, length of the queue at gating entries, number of vehicles inside-and-outside the reservoir, and emission caused by (NOx) and (CO_2). While emissions are not part of the control scheme, we found it interesting to include these factors to investigate the effect of gating

on them more broadly. In our accumulation-based model framework, the total time spent on each route i is calculated as

$$TTS_i(t) = \int_0^t \left(n_{IL,i}(\tau) + n_i(\tau)\right) d\tau, \tag{22}$$

where $n_{IL,i}(\tau)$ is the accumulation of inbound link i. Note that $n_{IL,1}(\tau) = 0$ because the first route corresponds to internal trips and the accumulation of the bypass $n_f(\tau)$ must be added in the calculation of $TTS_2(t)$.

In the following, we compare the results of Uncontrolled (UC) and gating-based Perimeter Control (PC). For the PI controllers, proportional and integral gains are tuned based on a trial and error method and saturation limits are imposed on the input flows with the values given in Table 2.

Table 2: Values of the proportional and integral gains and saturation limits on input for PI controller design.

Parameter	**Value**	**Unit**
Sampling time (T_s)	1	s
Proportional gains (k_P)	[0.6 0.6]	-
Integral gains (k_I)	[0.05 0.05]	-
Minimum input flow ($u_{\min}$)	[0.1 0.1]	veh/s
Maximum input flow ($u_{\max}$)	[3 3]	veh/s

5.1. Case I: Increasing the Internal Trip Volume

In this case, a congestion scenario is created by increasing internal trip demand inside the reservoir. The related demand pattern is presented in Fig. 7.

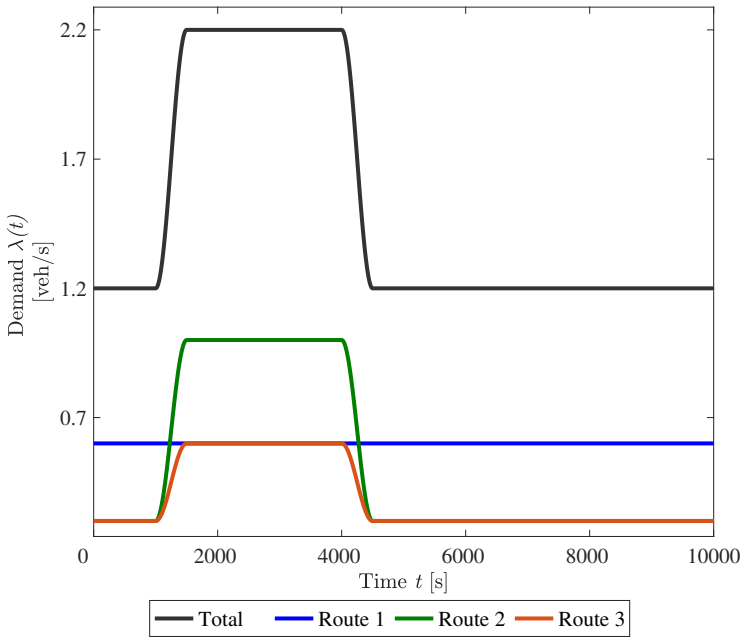

Fig. 7: Inflow demand profile used in case I.

As these trips have full priority and are not limited by the entry flow function, accumulation n quickly exceeds the critical accumulation n_c which leads to reduced outflows.

Fig. 8 shows the travel time profiles for route 2. Fig. 8 (a) shows the travel time on the bypass and route 2 for the uncontrolled case and Fig. 8 (b) shows the same for the control case. During congestion periods, the travel time for the uncontrolled and control cases matches with the bypass travel time (T_p^m). It shows that the proposed modeling framework works as expected for user equilibrium. The detailed analysis of the travel times is given in Appendix B.

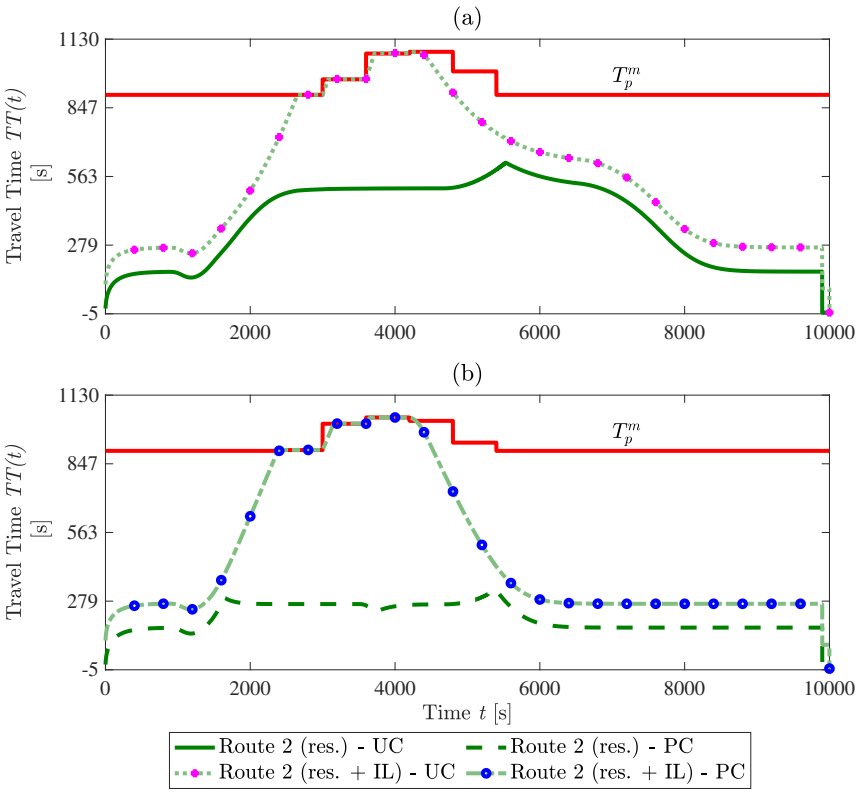

Fig. 8: Travel time evolution of route 2 inside and outside the reservoir.

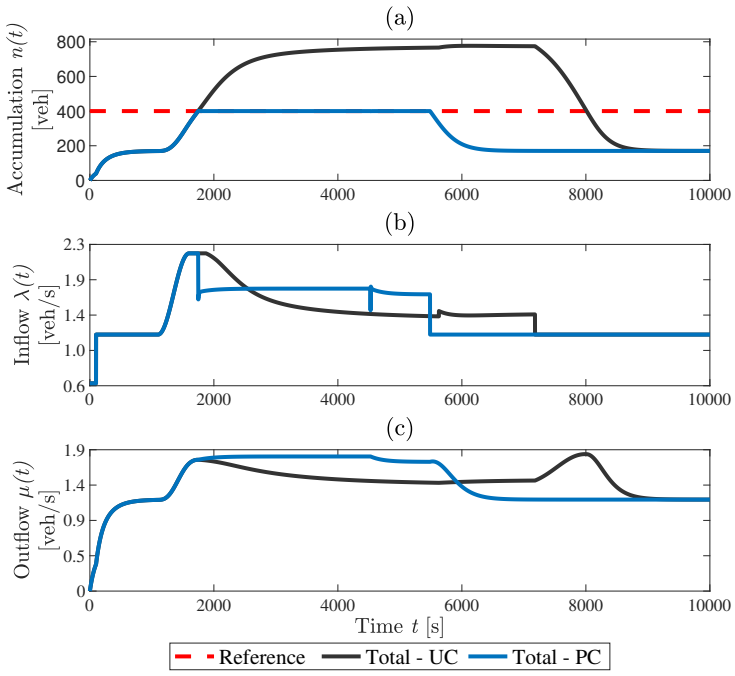

Fig. 9: Total accumulation (a), inflow (b), and outflow (c) inside the reservoir.

In the uncontrolled case, congestion appears in the reservoir, as shown in Fig. 9. To alleviate it the perimeter gating control scheme with the PI controller is utilized, as described in Section 4. The objective of the controller is to track n to n_c. Fig. 9 (a) shows the closed-loop performance of the uncontrolled and control cases. During the network loading period, both cases show the same performance. Once demand starts increasing, the uncontrolled case drives the reservoir into a congested state, whereas the PI controllers maintain accumulation at n_c.

Fig. 9 (b) and (c) shows the corresponding input and output flows for the uncontrolled and controlled cases, respectively. For the initial period, the inflow and outflow are the same. Once the total accumulation reaches n_c, the controller suddenly decreases the inflows. Due to the low inflow and high outflow, the mean speed increases. After that, the controller keeps the inflow constant until there is no change in demand. At time 4425 s demand decreases and thus we can see

a sharp decrease in the inflow for a short duration.

Fig. 10 shows the profiles of accumulation, inflow, and outflow for each route. Fig. 10 shows (a) that in the controlled case during the congestion period, route 2 has a higher accumulation due to the highest demand and trip length.

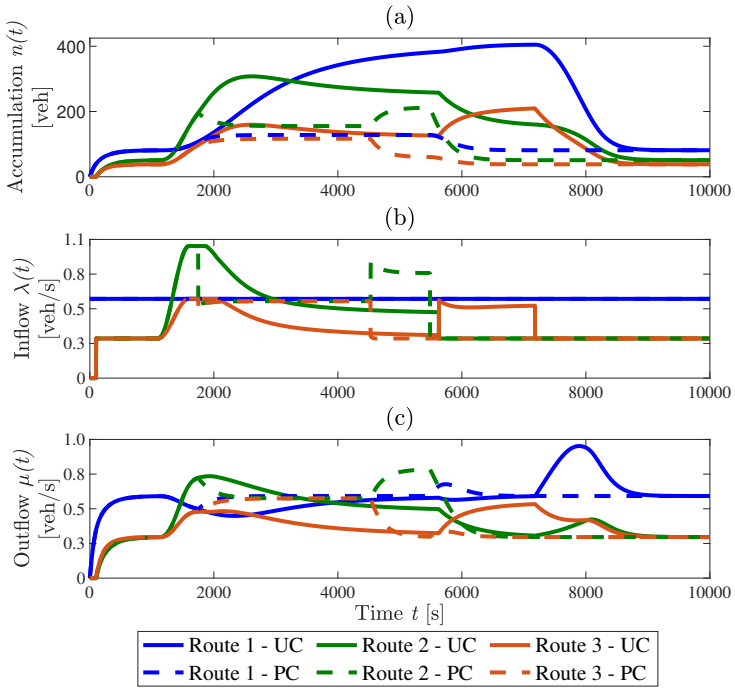

Fig. 10: Accumulation (a), inflow (b), and outflow (c) for each route inside the reservoir.

Fig. 10 (b) and (c) shows the inflow and outflow profiles for all routes. To achieve the desired reference value, the controller balances the inflow on routes 2 and 3. This results in a different accumulation on both routes inside the perimeter when comparing the uncontrolled and controlled cases. This is very pronounced here because routes 2 and 3 have different lengths.

From the above figures, it is clear that perimeter gating controllers help to keep accumulation at the desired value. However, it modifies traffic behavior outside the perimeter because we properly account for users switching routes to maintain DUE as queues increase at the gating entries. Fig. 11 shows the

evolution of accumulation of vehicles on each route outside the reservoir and on the bypass. The length of the queue on route 2 is increased due to the controller that limits access to this route after 2000 s. For route 3, there is smaller queue in the perimeter control case, due to the increase in inflow and outflow. Route 3 is shorter so it benefits from the control on route 2 to increase its share inside the reservoir and then allows higher inflow. Regarding the bypass, almost the same number of vehicles takes this alternative in both the uncontrolled and control cases. But in the control case, switching to the bypass occurs sooner than in the uncontrolled case when the gating on route 2 becomes effective.

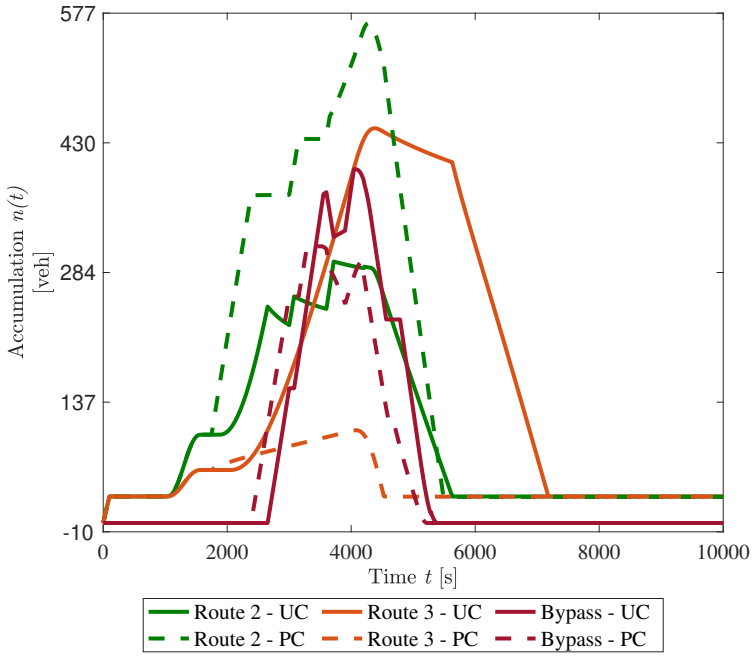

Fig. 11: Accumulation of vehicles on the inbound links and bypass.

Fig. 12 depicts the total time spent to reach the destination. With the perimeter gating control, the total TTS in the network is improved by 31.13% in comparison to the uncontrolled case. This is a positive side-effect as the perimeter control is designed to optimize the reservoir state, not the full system. It can be seen that this improvement is mostly due to routes 1 and 3. As

a general rule, improving the TTS of a given route mainly depends on the improvement of this route's outflow, because usually the demand for this route (its inbound link inflow) cannot be modified. But this is also true for route 2, where part of the inbound link inflow is diverted to the bypass because of the DUE discipline. In Fig. 10 (b), we see that once n reaches n_c, the controller reduces the inflows of routes 2 and 3. As a result, the queue starts increasing at IL. But this does not necessarily mean that more users will switch to the bypass because the travel time in the reservoir is better due to improved traffic conditions (see Fig. B.29 in Appendix B). As shown in (11), the switch ratio to the bypass is directly governed by the outflow of route 2. Hence, the slight worsening and then slight improvement of the TTS of route 2 (see in Fig. 12) are fully explained by the worse and then better outflow of this route in the control case.

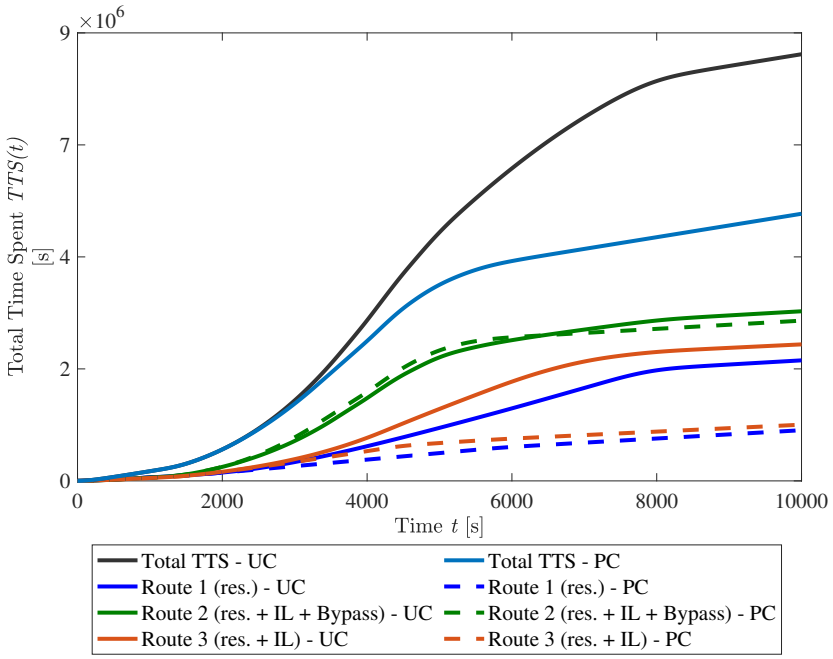

Fig. 12: Total time spent by the vehicles in whole network (reservoir + inbound link + bypass).

Fig. 13 (a) shows the emission level for NO_x and CO_2 in the reservoir. For the control case during the congestion period, the instantaneous emission levels are quite similar. This is because of the emission reduction gained from increased mean speed and the increase in distance traveled at each time-step due to better traffic conditions. After the congestion period, the emission level falls, which reduces the total emission for the perimeter control case. Thus, reducing congestion through optimal gating has a positive side-effect in terms of emission. Over all, the controller reduces NO_x by 1.52 kg and CO_2 by 223.06 kg, with significant improvement in the mean speed (see Fig. 13 (b)).

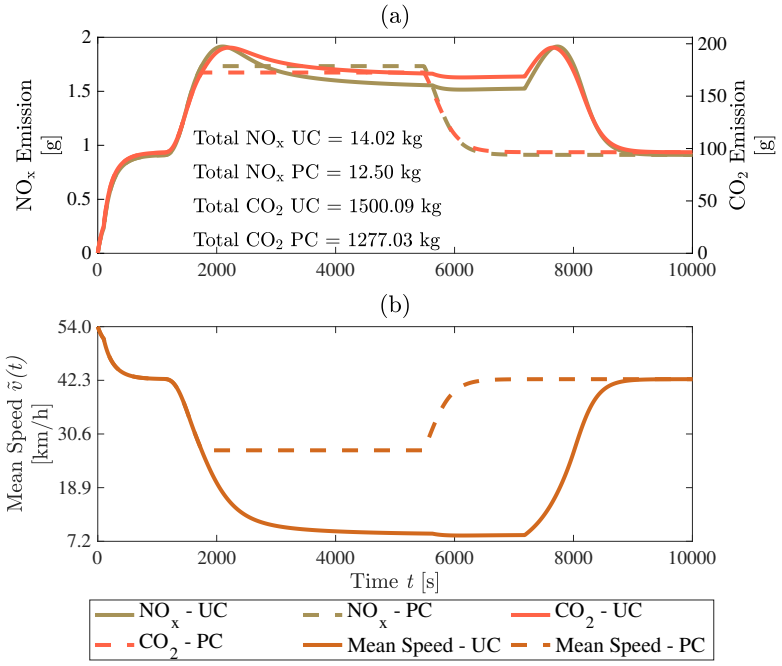

Fig. 13: Emission level of NO_x and CO_2 (a) and mean speed (b) in the reservoir.

5.2. Case II: Outflow Restriction on Route 2

In this case, congestion occurs because outflow is limited on route 2 ($q_{\text{out},2}$) by 0.6 veh/s, mimicking what will happen in the case of an accident, for example. There is no restriction on the maximum outflows of routes 1 and 3. Fig. 14 shows the route-wise and total input demand considered for this case. Demand

profiles are given such that controller performance can be tested for congested (from time 1000 to 4500 s) and free-flow traffic states.

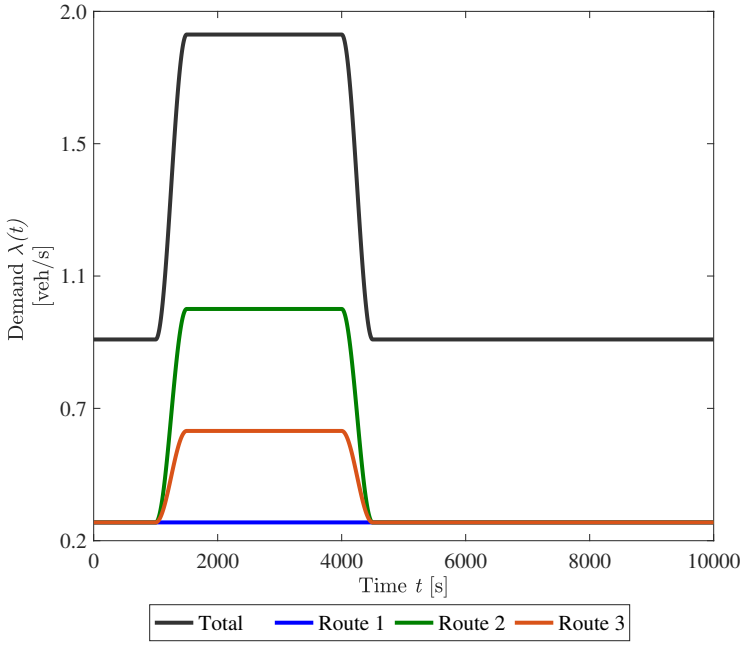

Fig. 14: Inflow demand profile used in case II.

Fig. 15 (a) depicts the response of uncontrolled and perimeter gating control cases in terms of accumulation. It can be seen that from time 1000 s, as total demand starts increasing the total accumulation of vehicles also continues increasing. In the control case, the PI controller keeps congestion at n_c, by manipulating the inflows at the perimeter, as shown in Fig. 15 (b). To keep n at n_c, outflow at the exit is maintained at the same value as inflow (see Fig. 15 (c)). For the uncontrolled case, around 5500 s, we can see the bump in the total outflow due to the discharge of vehicles stored in the reservoir once traffic conditions are improved after the demand peak. It is interesting to observe that there is no bump in the perimeter control case because of the improved outflow during the onset of demand.

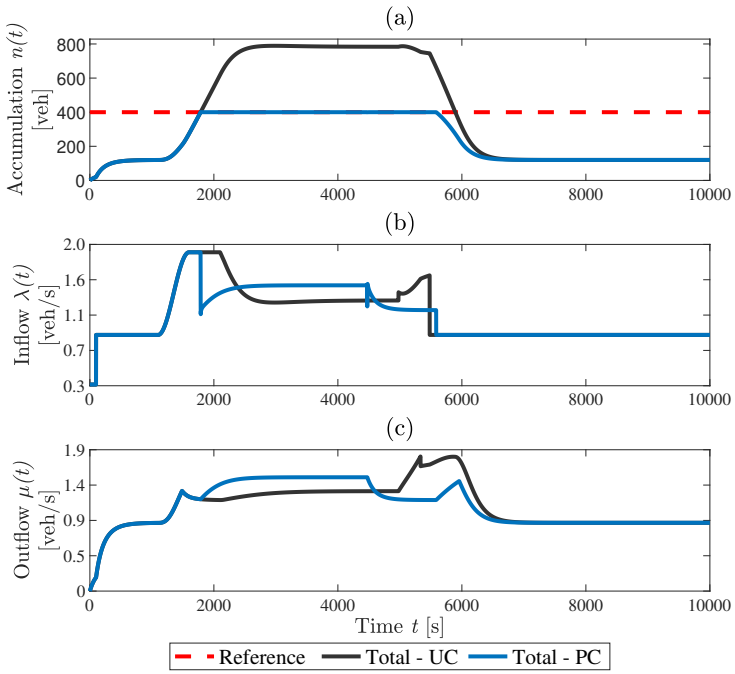

Fig. 15: Total Accumulation (a), inflow (b), and outflow (c) inside the reservoir.

Fig. 16 (a) shows the route-wise accumulation response of the uncontrolled and controlled cases. Due to the restriction on $q_{\text{out},2}$ of 0.6 veh/s, we can see that as the controller reaches n_c, inflows $q_{\text{in},2}$ and $q_{\text{in},3}$ suddenly decrease to keep the total accumulation at the desired value (see Fig. 16 (b)). Consequently, $q_{\text{out},2}$ and $q_{\text{out},3}$ reach steady state at 0.6 veh/s (see Fig. 16 (c)). The $q_{\text{in},1}$ remains unchanged as it is fixed to a constant flow. However, we can see an improvement in the $q_{\text{out},1}$ during the high demand period to keep n at n_c.

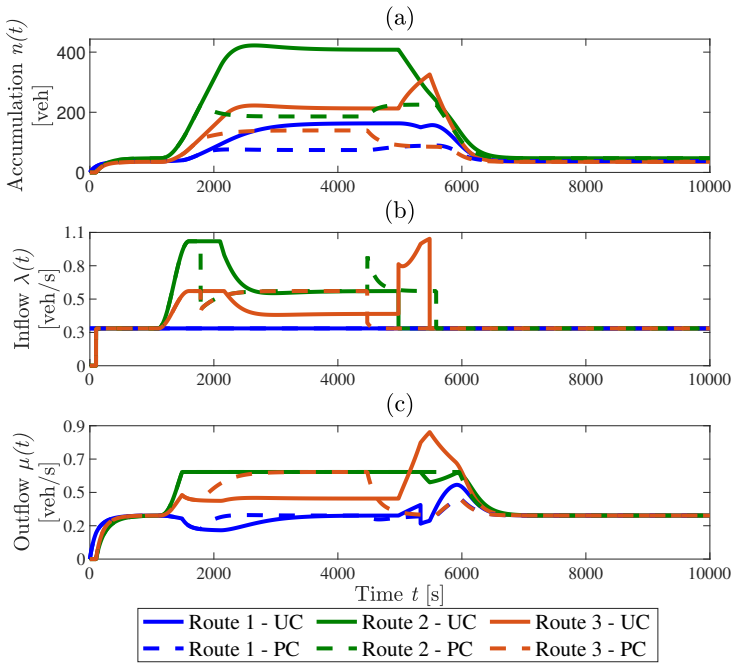

Fig. 16: Accumulation (a), inflow (b), and outflow (c) for each route inside the reservoir.

Fig. 17 shows the consequence of control in the form of queues at the perimeter and an accumulation of vehicles on a bypass. In this case, as expected during the congestion period, route 2 has a large queue in the control case due to the restriction on the outflow. The accumulation on the bypass is exactly the same in the uncontrolled and control cases due to the same outflow in both cases (see our previous explanation about Fig. 12). Route 3 has a smaller queue in the control case due to the increase in its inflow and outflow.

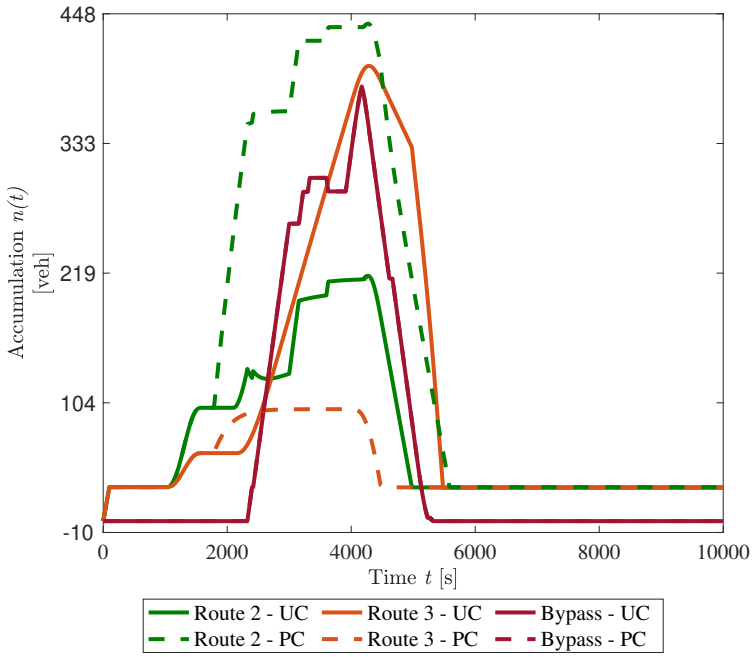

Fig. 17: Accumulation of vehicles on the inbound links and the bypass.

Fig. 18 depicts the total time spent for the vehicles traveling on each route. For the perimeter control, it can be seen that: (a) the TTS of routes 1 and 3 are reduced by 36.84% and 44.89%, respectively (b) but the TTS of route 2 is relatively unchanged because similar outflows are observed in both the uncontrolled and control cases (see also the explanation of Fig. 12).

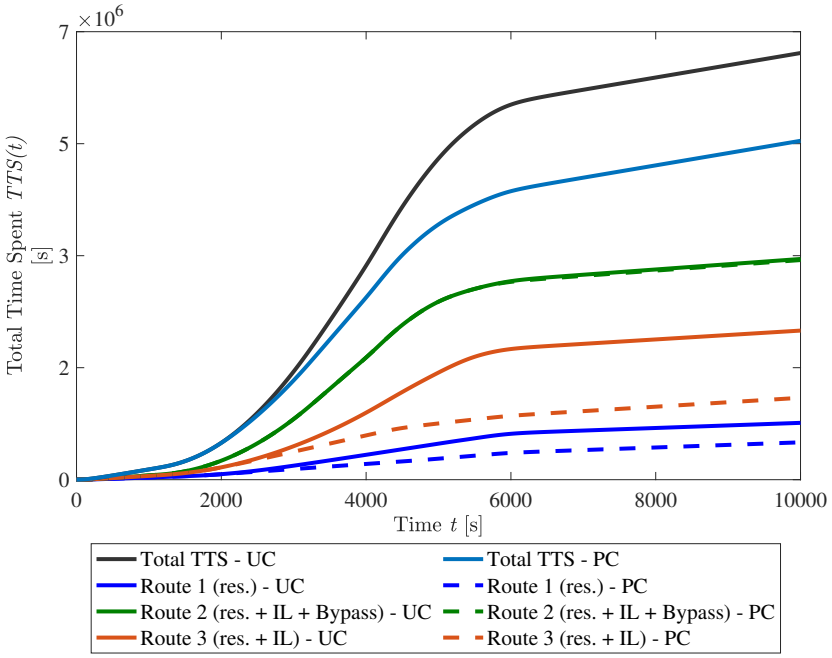

Fig. 18: Total time spent by the vehicles in the whole network (reservoir + inbound link + bypass).

Fig. 19 (a) shows the emission levels of NO_x and CO_2, respectively. It can be seen that the instantaneous emission levels of NO_x and CO_2 are quite similar in both the uncontrolled and control cases, though slightly higher during congestion in the control case. As explained previously for Fig. 13 (a), this is due to a compensation effect between the increased mean speed and the increase in the distance traveled at each time-step.

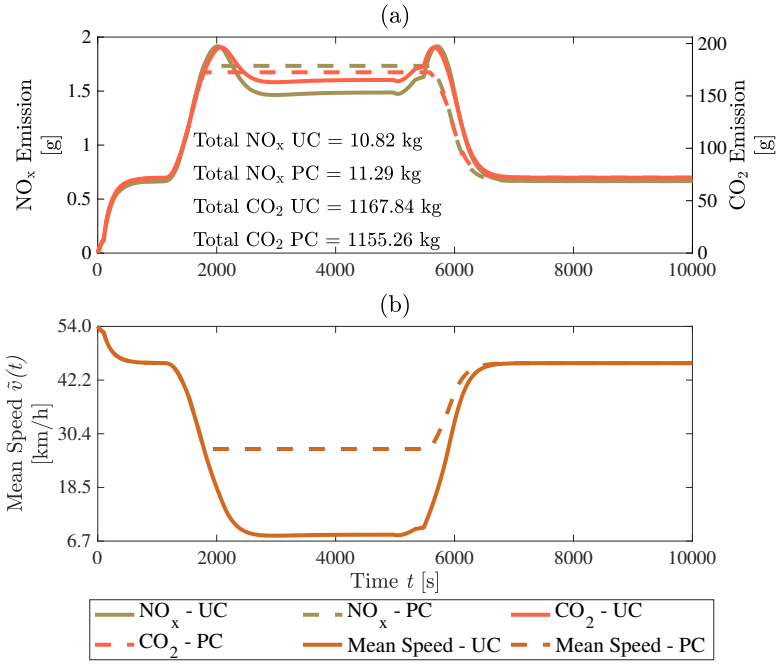

Fig. 19: Emission level of NO_x and CO_2 (a) and mean speed (b) in the reservoir.

5.3. Case III: Outflow Restriction on Route 3

In this case, congestion is created by imposing the restriction of 0.65 veh/s on ($q_{\text{out},3}$), whereas there is no restriction on the maximum outflow rate of routes 1 and 2. Fig. 20 shows the input demand profile used in this case. The main difference with the previous case is that route 3 has no alternative and users will have to go through the reservoir whatever the action of the gating scheme.

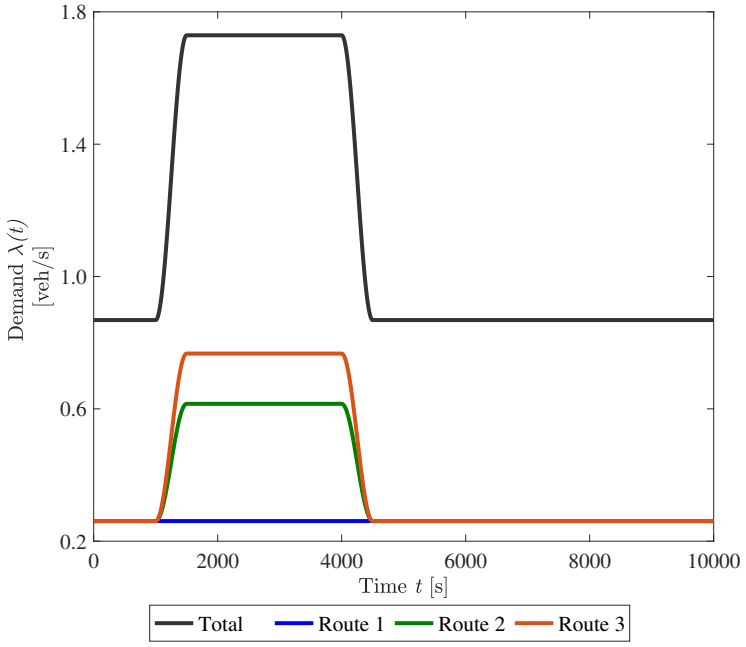

Fig. 20: Inflow demand profile used in case III.

Fig. 21 shows the evolution of the response of the uncontrolled and controlled cases.

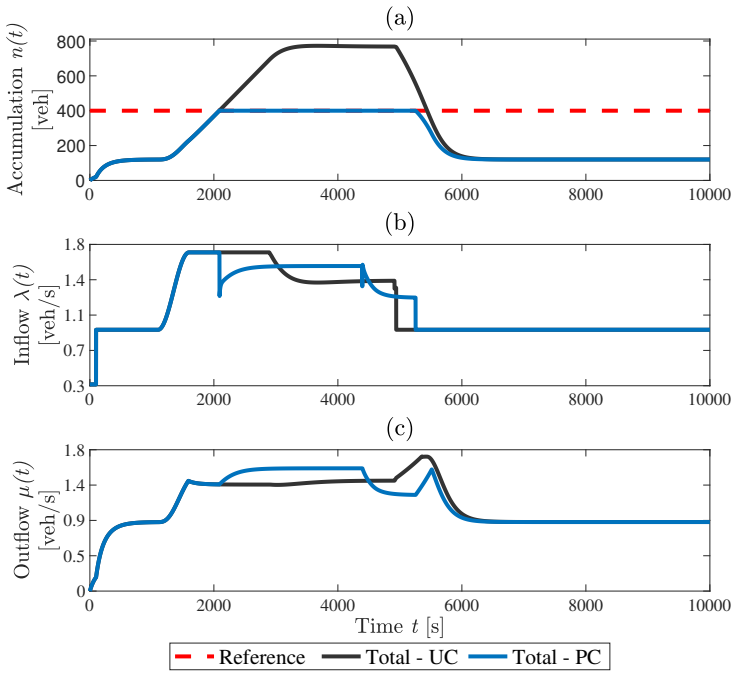

Fig. 21: Total Accumulation (a), inflow (b), and outflow (c) inside the reservoir.

Fig. 22 (a) shows the accumulation of vehicles on each route. It can be seen that during the congestion period (in controlled case) route 2 has more accumulation in comparison to route 3 due to the increase in inflow ($q_{\text{in},2}$) and the mean speed in the reservoir. Fig. 22 (b) and (c) shows the inflow and outflow profiles of each route.

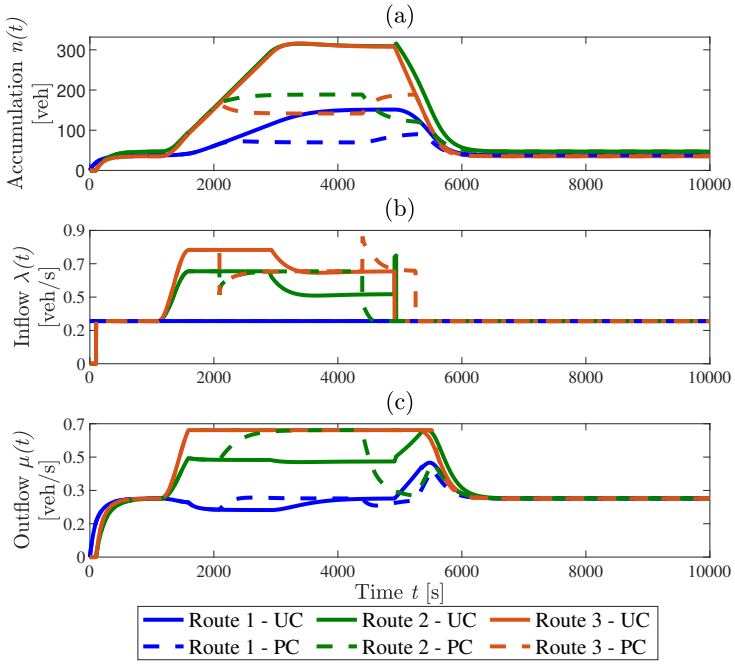

Fig. 22: Accumulation (a), inflow (b), and outflow (c) profiles of each route inside the reservoir.

Fig. 23 illustrates the impact of perimeter control on the queues for routes 2 and 3 and accumulation on the bypass. The effect of the restriction on $q_{\text{out},3}$, is that we can see a long queue during the congestion period for the control case. Due to the increase in $q_{\text{out},2}$, route 2 has a smaller queue and no vehicle takes the bypass.

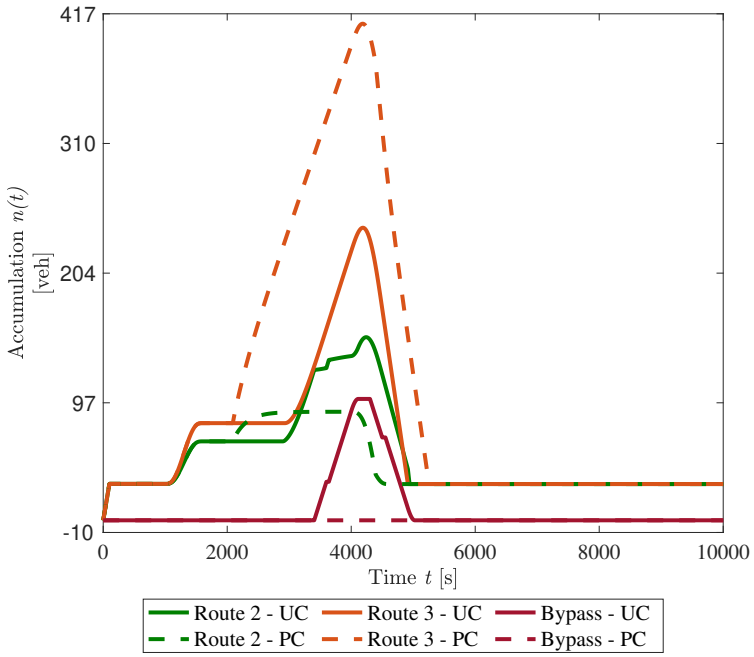

Fig. 23: Accumulation of vehicles on the queues and a bypass.

Fig. 24 shows the travel time spent on each route and the whole network. Due to the restriction on the outflow of route 3, the TTS for the uncontrolled and control cases is same. However, due to the increase in $q_{\text{out},2}$ in the control case, the overall TTS of routes 1 and 2 is reduced by 29.57% and 28.86%, respectively.

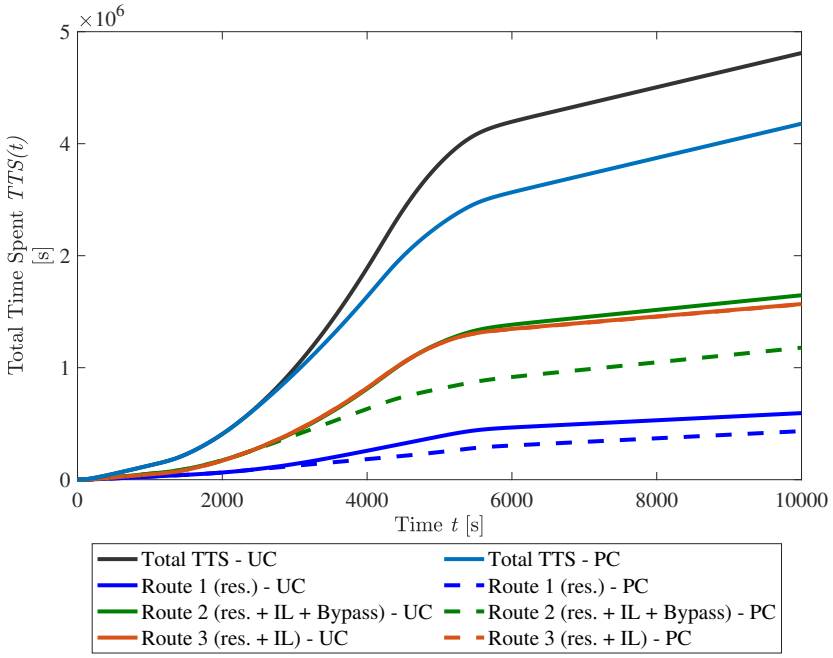

Fig. 24: Total time spent by the vehicles in whole network (reservoir + inbound link + bypass).

Fig. 25 shows the instantaneous emission levels of NO_x and CO_2. In this scenario, similar emission levels are observed in both the uncontrolled and control cases, because of the compensation effect previously described for Fig. 13 and Fig. 19.

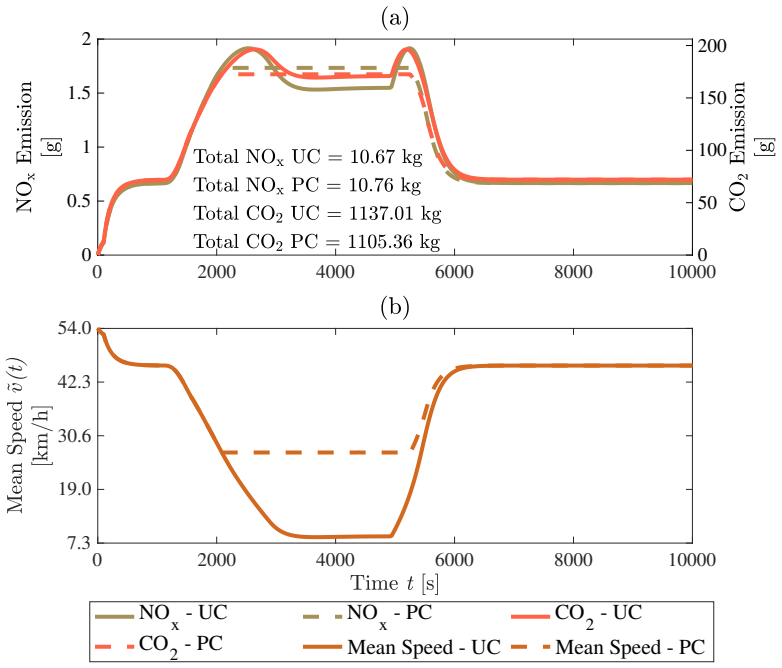

Fig. 25: Emission level of NO_x and CO_2 (a) and mean speed (b) in the reservoir.

Table 3 gives the summary of all the indicators for all three test cases considering the uncontrolled and perimeter control situations. The values given in the table are calculated for the whole simulation time (10000 s) in the form of percentage (%) with respect to the uncontrolled case. The values indicated in red show a negative effect, values in green show a significant positive effect, and the values in blue show minor positive or negative effects of the control.

Case	Queue		Accumulation	Total Time Spent				Emission NO_x				Emission CO_2				Mean Speed	
	R_2	R_3	Bypass	R_1	R_2	R_3	Total	Res.	Queue	Bypass	Total	Res.	Queue	Bypass	Total	Res.	Queue
I	60.27	-70.55	13.52	-54.14	-0.58	-54.60	-31.13	-10.83	-5.24	-13.52	-9.43	-14.87	-4.30	-13.52	-10.91	61.55	18.40
II	97.58	-54.50	0	-36.84	-0.34	-44.89	-20.56	4.32	0.73	0	1.40	-1.07	0.46	0	0.25	23.42	0.07
III	-13.18	65.35	-100	-29.57	-28.86	-0.10	-16.88	0.83	5.43	-100	-1.80	-2.78	5.88	-100	-3.46	15.09	-3.65

Table 3: Performance comparison of uncontrolled and perimeter gating control approach.

5.4. Emission Minimization

The previous analysis for all three cases shows that improving traffic conditions inside the reservoir also reduces the emission. It may also reduce the total emission in the system compared to the uncontrolled case because the supplementary total emission related to the vehicles re-routed on the bypass alternative with the longer distance is more than compensated by the reduction in the reservoir. An interesting question is whether it is possible to do even better for the total emissions in the system with gating? Designing a complete optimization framework is out of the scope of this study and is currently being investigated by the authors, but we give certain directions here. Let us first consider the reservoir, the instantaneous emission curves for NO_x and CO_2 are provided in Fig. 5. As the free-flow speed is 54 km/h, all the possible emission levels are represented by the decreasing left branches of both curves. Thus, minimizing instantaneous emission inside the reservoir consists in making the speed levels close to the free-flow one since travel distances are constant inside the reservoir. The extreme case would be to set the speed to $\tilde{v}_f$, but on looking at the MFD no inflow can enter. Naturally, the emissions are minimized inside the reservoir as they are equal to zero, but this will force all the vehicles to take a longer alternative and obviously significantly generate higher total emissions in the network. We also show that controlling the reservoir at n_c improves the total emission compared to the uncontrolled case. The question now is: is there a lower control value $n_{c,e}$ between zero and n_c that would further improve the total emission. To answer this question, we simply list different values for case III, see Fig 26 (a). Obviously, the lower $n_{c,e}$ gives the lower emission inside the reservoir because: (i) the more the mean speed increases and (ii) the more severe the gating becomes, the more vehicles take the alternative route, thereby reducing the demand to the reservoir for route 2. Likewise, it is not surprising that the emission outside the reservoir increases when $n_{c,e}$ decreases, because: (i) vehicles are queuing more to enter the reservoir, and (ii) more vehicles are taking the alternative, which increases their travel distance. What is interesting is to look at total emission. A global minimum is achieved when $n_{c,e} = 290$,

which is below the critical accumulation . Thus, a gating strategy can be implemented to minimize total emission in the network; however, determining the optimal $n_{c,e}$ value is challenging. Here, we only presented such a value based on trials for a given case. Fig 26(b) shows the total time spent for different $n_{c,e}$ values. It can be noted that when decreasing $n_{c,e}$ from n_c, the total TTS in the reservoir is reduced as we limit the inflow. The total TTS follows an opposite trend because of longer queues on inbound links and more vehicles on the bypass alternative with a longer distance to travel. Interestingly, the total TTS follows the same global trend as total emission with a minimum for $n_c = 290$. Therefore, more severe gating may be very effective at the global network scale: gains inside the reservoir that exclude the loss outside. The only but significant challenge is to define the optimal value of $n_{c,e}$ in practice. Appendix A shows the results for cases I and II. The optimal $n_{c,e}$ value for case I is the critical accumulation $n_{c,e} = 400$. For case II, the optimal value is $n_{c,e} = 290$.

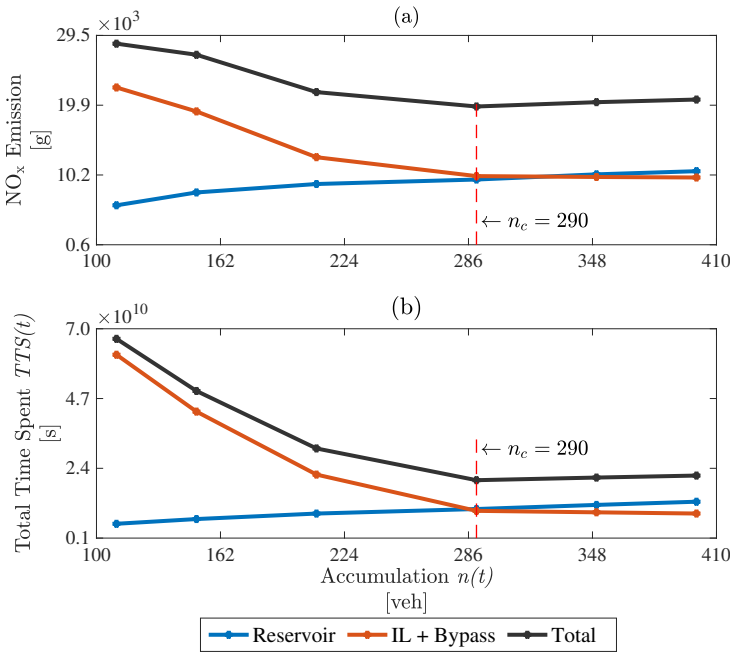

Fig. 26: Evolution of the total emission for different control thresholds ($n_{c,e}$) for case III.

6. Conclusion

This paper proposed a complete modeling framework to assess the global effect of gating control at the entries of an urban area. This framework combined a reservoir characterized by the accumulation-based MFD model, inbound links defined with the point-queue model, and bypass alternatives represented by piece-wise constant travel time functions corresponding to the steady-state approximation of the MFD model. The strength of this framework is its ability to determine the instantaneous path-flow distribution between reservoir and bypass routes following UE discipline. This permits controlling the full consequences of the gating strategy by considering that the demand to the reservoir may be elastic as users may favor switching their initial itinerary if travel times make some other alternative competitive. Considering this effect is paramount to provide a complete vision of full network functioning and provide a global assessment in terms of traffic efficiency and emission. The performance and impacts of the perimeter gating controller were tested in simulations of traffic congestion scenarios created by increasing internal trips and restricting the outflows. The results showed that the gating control scheme improves traffic conditions inside the perimeter with a small impact on the outside traffic conditions, because users make their route choice and reconsider the reservoir option. This keeps the queue at the reservoir gate at a reasonable size. In every case, the results of the perimeter gating controller were compared with a uncontrolled case. Comparative analysis showed that the gating control scheme improves the total time spent in the network and mean speed at the cost of a small increase in the queues at the inbound links. We showed that gating strategy can be used to minimize total emission in the network by using the PI controller to track an accumulation value lower than the critical accumulation. Determining this optimal value is very challenging and requires further analysis. The future goal of this research is to generalize the proper framework to account for multiple bypass routes and cities partitioned in multiple reservoirs with gating at all perimeter entries.

Acknowledgments

The research leading to these results has received funding from the European Research Council (ERC) under the European Union's Horizon 2020 research and innovation program (grant agreement No. 646592 – MAGnUM project).

Appendix A. Emission Minimization: Case I and II

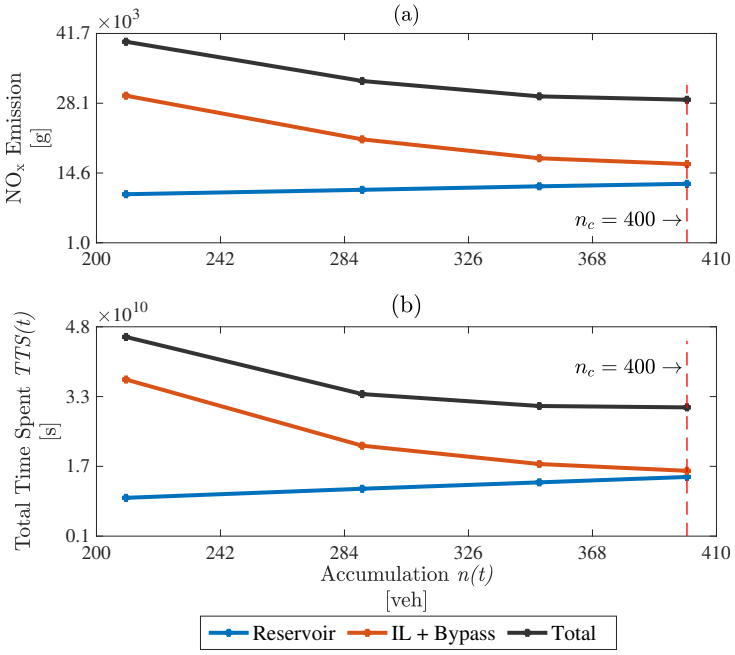

Fig. A.27: Evolution of the total emission for different control threshold ($n_{c,e}$) for case I.

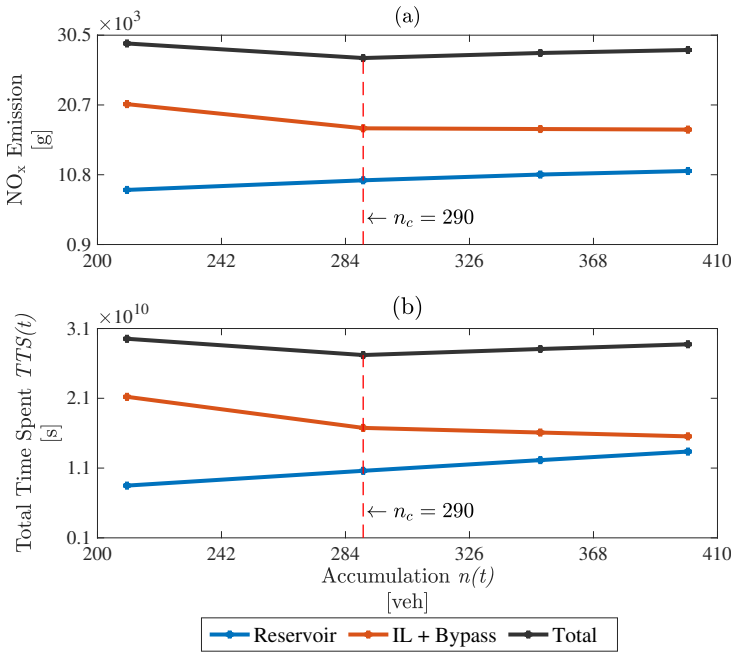

Fig. A.28: Evolution of the total emission for different control thresholds ($n_{c,e}$) for case II.

Appendix B. Exact Predictive Travel Time

We present here the evolution of the exact predictive travel time $T_{IL,i}(t) + T_i(t + T_{IL,i}(t))$ for vehicles entering route 2 and 3 at t ($i = 2, 3$). This travel time is composed by the exact predictive travel time on the inbound link $T_{IL,i}$ and in the reservoir T_i, as defined in Section 3.3.

Fig. B.29 shows the exact predictive travel times in case I. It can be seen that the gating control reduces travel time for routes 2 and 3 inside the reservoir. This is due to the increased mean speed in the reservoir. For route 2 (reservoir + inbound link), the travel time matches with T_p^m in the uncontrolled and control cases. For route 3 (reservoir + inbound link) in the control case, the travel time is decreased due to the increase in inflow and outflow. This illustrates the DUE discipline in both the uncontrolled and control cases. However, in the control case switching time to the bypass is sooner in comparison to the uncontrolled

case. The travel time for the uncontrolled and control cases is different due to the diversion of some vehicles on the bypass (see Fig. 11.)

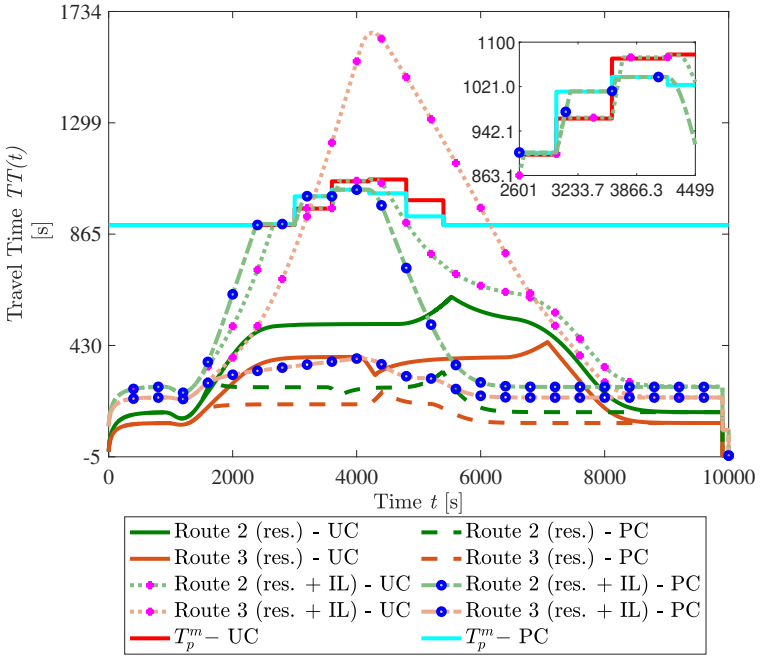

Fig. B.29: Exact predicted travel time for vehicles inside the reservoir and in the inbound links for the case I.

Fig. B.30 shows the profiles of exact predictive travel times in case II. It can be seen that the total travel time for route 2 (reservoir + inbound link) in both uncontrolled and control cases are identical. As discussed in Section 5.2, gating control is unable to improve the global situation of route 2 (reservoir + inbound link) due to the exogenous limitation on the outflow of this route. This explains why the total travel time in the control case is same as the uncontrolled case even if the travel time in the reservoir is notably reduced (congestion is moved from inside to outside the perimeter). The travel time on route 3 for vehicles in the inbound link is short in the control case due to the smaller queue and increased inflow and outflow.

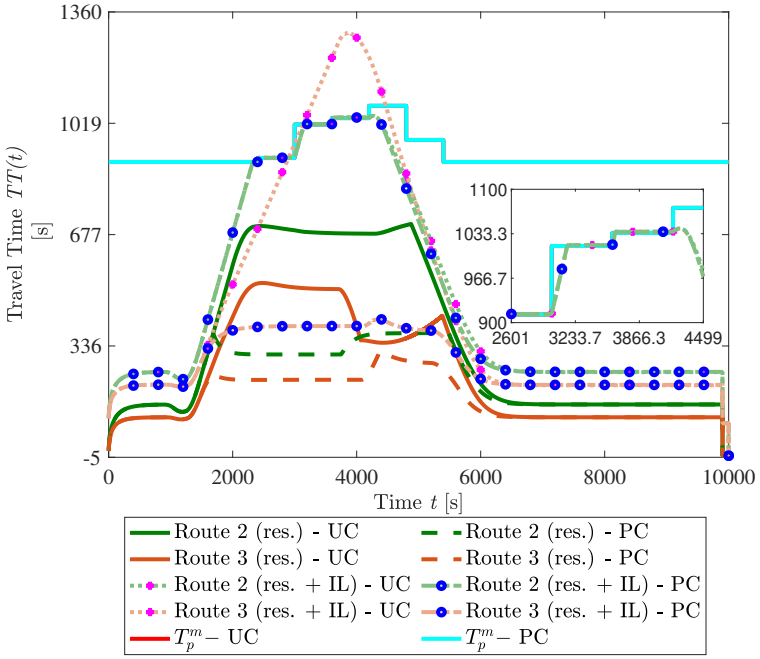

Fig. B.30: Exact predicted travel time for vehicles inside the reservoir and in the inbound links for the case II.

Fig. B.31 shows the exact predicted evolution of travel time in case III. In this case, as the outflow limitation is on route 3, a similar phenomenon is observed for this route to that of route 2: total travel time (reservoir + inbound link) is the same in both uncontrolled and control cases. In the control case, vehicles on route 2 (reservoir + inbound link) experience a shorter travel time than for the uncontrolled case. As the travel time of vehicles on route 2 is shorter than T_p^m, no vehicle is diverted to the bypass and therefore there is no accumulation on a bypass.

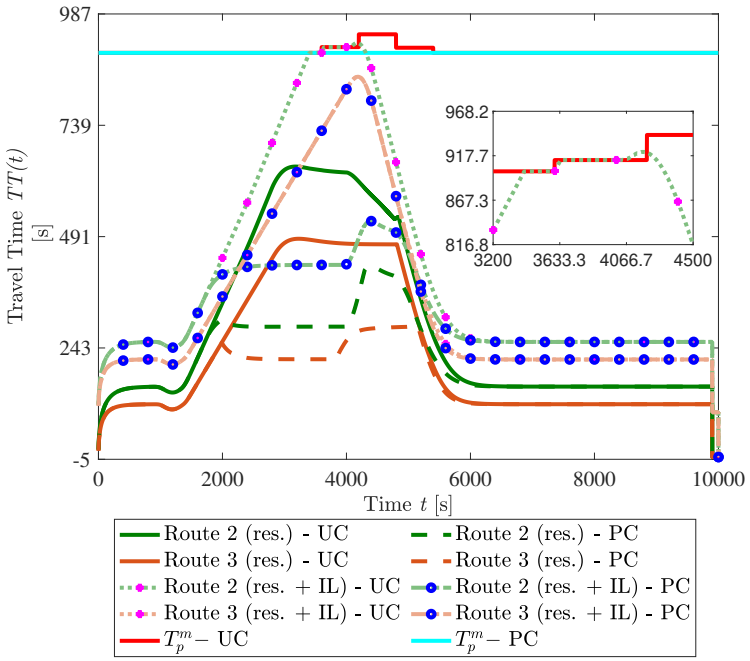

Fig. B.31: Exact predicted travel time for the reservoir and the inbound links for case III.

Appendix C. Output Production MFD

We present here the total exit production of the reservoir versus total accumulation for the uncontrolled and perimeter gating control cases. The exit production is calculated as the sum of all route outflows multiplied by their trip length inside the reservoir:

$$P_{\text{out}}(t) = \sum_{i=1}^{N} L_i q_{\text{out},i}(t), \tag{C.1}$$

where $N = 3$ is the number of routes inside the reservoir. $P_{\text{out}}(t)$ shows the performance of the network under free-flow and congestion states.

Fig. C.32 illustrates the evolution of $P_{\text{out}}(t)$ versus $n(t)$ in case I. For the uncontrolled case, we observe over-saturation in the reservoir as the accumulation $n(t)$ exceeds the critical accumulation n_c. The exit production decreases during congestion due to the drop in mean speed, as the result of the high

number of internal trips. We also notice a clockwise hysteresis loop during the congestion period. This loop is explained by the reservoir dynamics with different trip lengths: during recovery, the lower exit production is due to the lower outflow on route 2 which has a long trip length, see also Fig. 16. It can be seen that gating controller limits the accumulation of vehicles from going beyond the reference value n_c.

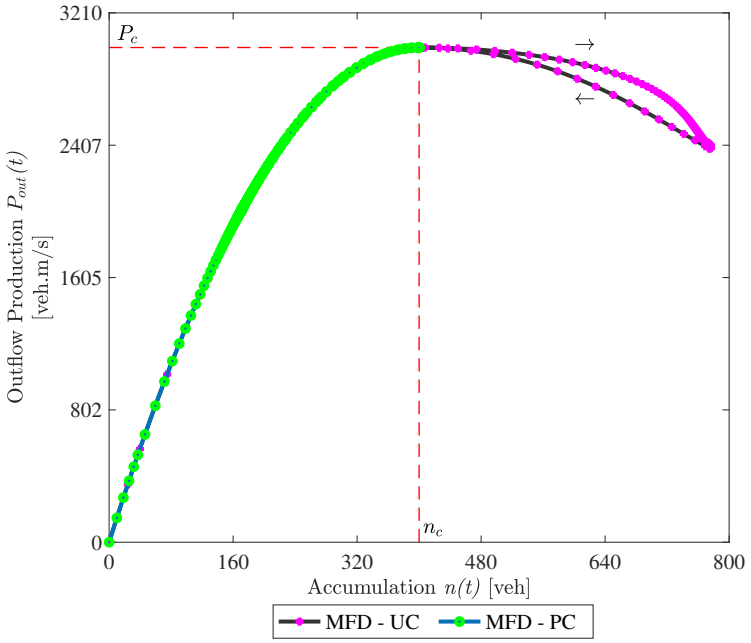

Fig. C.32: Production MFD at the exit of reservoir for case I.

Fig. C.33 shows the evolution of $P_{\text{out}}(t)$ versus $n(t)$ in case II. For the uncontrolled case, we observe a large counter-clockwise hysteresis loop, which is due to the differences in traffic dynamics between the onset and offset of congestion. During the loading of the reservoir at the beginning of the simulation, the outflow limitation on route 2 also impacts the outflow of other routes because of the outflow inter-dependency relationships described in (6). Basically, these relationships represent the effect of the drop in mean speed during congestion, which applies to all the routes equivalently. This explains the low and almost constant exit production during the onset of congestion. But once the

route flow demands decrease after $t = 5000$ s, the reservoir can recover: the mean speed increases and so does the outflow of routes 1 and 3 to discharge the vehicles inside the reservoir, see also Fig. 22. This is the reason for the higher exit production during the offset of congestion. Note that the recovery process is possible due to our assumption of a maximum outflow demand in over-saturation regime, see (7a). More details can be on this in Mariotte et al. (2017); Mariotte and Leclercq (2018). For the control case, however, the total accumulation is maintained at n_c during recovery, so that the hysteresis loop observed is much smaller.

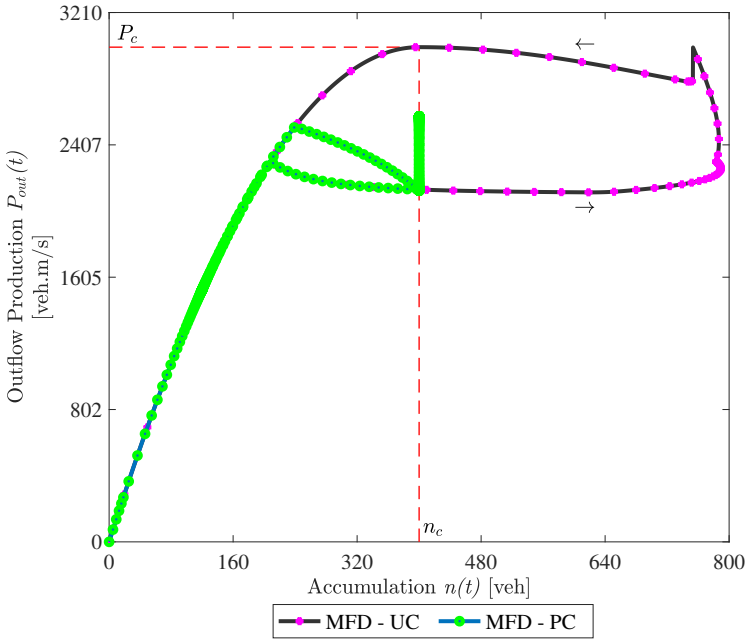

Fig. C.33: Production MFD at the exit of reservoir for case II.

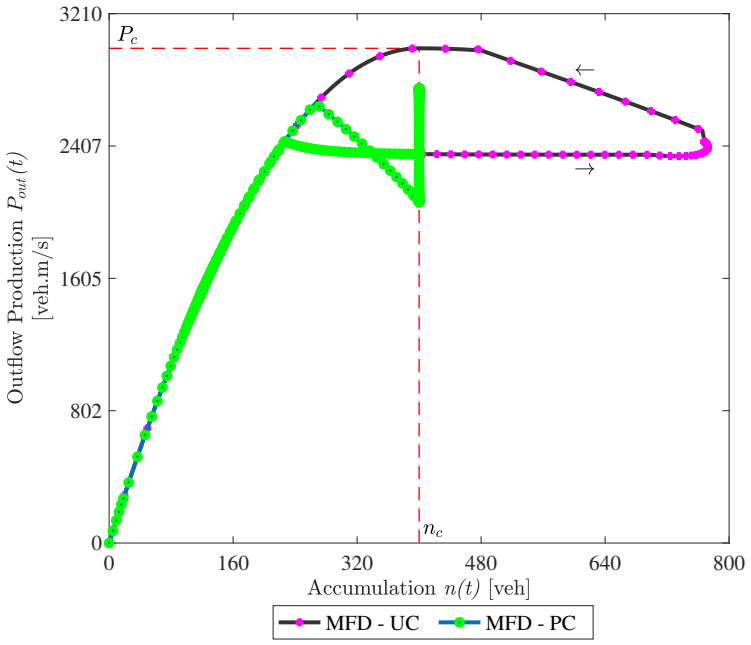

Fig. C.34: Production MFD at the exit of the reservoir for the case III.

Fig. C.34 shows the evolution of $P_{\text{out}}(t)$ versus $n(t)$ in case III. Because the mechanism of outflow limitation on route 3 is very similar to the limitation in the previous case II, we also observe quite a similar pattern in this case. Indeed, the counter-clockwise hysteresis loop in uncontrolled case is due to the low outflow of all the routes during the onset of congestion, and the higher outflow discharge once the reservoir recovers. As in case II, the controller keeps the total accumulation close to n_c, which explains the smaller hysteresis pattern observed in this case.

References

References

Aalipour, A., Kebriaei, H., Ramezani, M., 2018. Robust traffic flow control in networks with nonlinear MFD dynamics. 97th Annual Meeting TRB, Washington D.C.

Aboudolas, K., Geroliminis, N., 2013. Perimeter and boundary flow control in multi-reservoir heterogeneous networks. Transportation Research Part B: Methodological 55, 265–281.

Ampountolas, K., Zheng, N., Geroliminis, N., 2014. Perimeter flow control of bi-modal urban road networks: A robust feedback control approach. In: Control Conference (ECC), 2014 European. IEEE, pp. 2569–2574.

Ampountolas, K., Zheng, N., Geroliminis, N., 2017. Macroscopic modelling and robust control of bi-modal multi-region urban road networks. Transportation Research Part B: Methodological 104, 616–637.

Daganzo, C. F., 2007. Urban gridlock: Macroscopic modeling and mitigation approaches. Transportation Research Part B: Methodological 41 (1), 49–62.

Daganzo, C. F., Gayah, V. V., Gonzales, E. J., 2011. Macroscopic relations of urban traffic variables: Bifurcations, multivaluedness and instability. Transportation Research Part B: Methodological 45 (1), 278–288.

Ding, H., Guo, F., Zheng, X., Zhang, W., 2017. Traffic guidance–perimeter control coupled method for the congestion in a macro network. Transportation Research Part C: Emerging Technologies 81, 300–316.

Frejo, J. R. D., Núñez, A., De Schutter, B., Camacho, E. F., 2014. Hybrid model predictive control for freeway traffic using discrete speed limit signals. Transportation Research Part C: Emerging Technologies 46, 309–325.

Geroliminis, N., 2015. Cruising-for-parking in congested cities with an MFD representation. Economics of Transportation 4 (3), 156–165.

Geroliminis, N., Daganzo, C. F., 2008. Existence of urban-scale macroscopic fundamental diagrams: Some experimental findings. Transportation Research Part B: Methodological 42 (9), 759–770.

Geroliminis, N., Haddad, J., Ramezani, M., 2013. Optimal perimeter control for two urban regions with macroscopic fundamental diagrams: A model pre-

dictive approach. IEEE Transactions on Intelligent Transportation Systems 14 (1), 348–359.

Godfrey, J., 1969. The mechanism of a road network. Traffic Engineering & Control 8 (8).

Haddad, J., 2015. Robust constrained control of uncertain macroscopic fundamental diagram networks. Transportation Research Part C: Emerging Technologies 59, 323–339.

Haddad, J., 2017. Optimal perimeter control synthesis for two urban regions with aggregate boundary queue dynamics. Transportation Research Part B: Methodological 96, 1–25.

Haddad, J., Mirkin, B., 2017. Coordinated distributed adaptive perimeter control for large-scale urban road networks. Transportation Research Part C: Emerging Technologies 77, 495–515.

Haddad, J., Ramezani, M., Geroliminis, N., 2013. Cooperative traffic control of a mixed network with two urban regions and a freeway. Transportation Research Part B: Methodological 54, 17–36.

Haddad, J., Shraiber, A., 2014. Robust perimeter control design for an urban region. Transportation Research Part B: Methodological 68, 315–332.

Haddad, J., Zheng, Z., 2018. Adaptive perimeter control for multi-region accumulation-based models with state delays. Transportation Research Part B: Methodological.

Hajiahmadi, M., Haddad, J., De Schutter, B., Geroliminis, N., 2015. Optimal hybrid perimeter and switching plans control for urban traffic networks. IEEE Transactions on Control Systems Technology 23 (2), 464–478.

Hajiahmadi, M., Knoop, V. L., De Schutter, B., Hellendoorn, H., 2013. Optimal dynamic route guidance: A model predictive approach using the macroscopic

fundamental diagram. In: Intelligent Transportation Systems-(ITSC), 2013 16th International IEEE Conference on. IEEE, pp. 1022–1028.

Keyvan-Ekbatani, M., Carlson, R. C., Knoop, V. L., Hoogendoorn, S. P., Papageorgiou, M., 2016. Queuing under perimeter control: Analysis and control strategy. In: Intelligent Transportation Systems (ITSC), 2016 IEEE 19th International Conference on. IEEE, pp. 1502–1507.

Keyvan Ekbatani, M., Gao, X., Gayah, V., Knoop, V. L., 2016. Combination of traffic-responsive and gating control in urban networks: Effective interactions. Proceedings of the 95th annual meeting of the TRB, Washington (USA), 10-14 Jan. 2016; Authors version.

Keyvan-Ekbatani, M., Kouvelas, A., Papamichail, I., Papageorgiou, M., 2012. Exploiting the fundamental diagram of urban networks for feedback-based gating. Transportation Research Part B: Methodological 46 (10), 1393–1403.

Keyvan-Ekbatani, M., Papageorgiou, M., Papamichail, I., 2014. Perimeter traffic control via remote feedback gating. Procedia-Social and Behavioral Sciences 111, 645–653.

Kim, S., Tak, S., Yeo, H., 2018. Investigating transfer flow between urban networks based on a macroscopic fundamental diagram. Transportation Research Record 2672 (20), 75–85.

Kouvelas, A., Saeedmanesh, M., Geroliminis, N., 2017a. Enhancing model-based feedback perimeter control with data-driven online adaptive optimization. Transportation Research Part B: Methodological 96, 26–45.

Kouvelas, A., Saeedmanesh, M., Geroliminis, N., 2017b. A linear formulation for model predictive perimeter traffic control in cities. IFAC-PapersOnLine 50 (1), 8543–8548.

Lamotte, R., Murashkin, M., Kouvelas, A., Geroliminis, N., 2018. Dynamic modeling of trip completion rate in urban areas with MFD representations. 97th Annual Meeting TRB, Washington D.C.

Leclercq, L., Paipuri, M., 2018. Hysteresis loops in macroscopic fundamental diagrams: the bottleneck effect during congestion peaks and its consequences for reservoir-based simulation. submitted to Transportation Research Part B: Methodological –, –.

Lejri, D., Can, A., Schiper, N., Leclercq, L., 2018. Accounting for traffic speed dynamics when calculating copert and phem pollutant emissions at the urban scale. Transportation Research Part D: Transport and Environment 63, 588–603.

Li, Y., Xu, J., Shen, L., 2012. A perimeter control strategy for oversaturated network preventing queue spillback. Procedia-Social and Behavioral Sciences 43, 418–427.

Lin, S., De Schutter, B., Xi, Y., Hellendoorn, H., 2011. Fast model predictive control for urban road networks via MILP. IEEE Transactions on Intelligent Transportation Systems 12 (3), 846–856.

Maciejowski, J. M., 2002. Predictive control: with constraints. Pearson education.

Mahmassani, H. S., Williams, J. C., Herman, R., 1984. Investigation of network-level traffic flow relationships: some simulation results. Transportation Research Record 971, 121–130.

Majid, H., Hajiahmadi, M., De Schutter, B., Abouaïssa, H., Jolly, D., 2014. Distributed model predictive control of freeway traffic networks: A serial partially cooperative approach. In: Intelligent Transportation Systems (ITSC), 2014 IEEE 17th International Conference on. IEEE, pp. 1876–1881.

Mariotte, G., Leclercq, L., 2018. MFD-based simulation: Spillbacks in multi-reservoir networks. 97th Annual Meeting TRB, Washington D.C.

Mariotte, G., Leclercq, L., 2019. Flow exchanges in multi-reservoir systems with spillbacks. Transportation Research Part B: Methodological 122, 327–349.

Mariotte, G., Leclercq, L., Laval, J. A., 2017. Macroscopic urban dynamics: Analytical and numerical comparisons of existing models. Transportation Research Part B: Methodological 101, 245–267.

Mohajerpoor, R., Saberi, M., Vu, H. L., Garoni, T. M., Ramezani, M., 2019. H_∞ robust perimeter flow control in urban networks with partial information feedback. Transportation Research Part B: Methodological.

Ni, W., Cassidy, M. J., 2019. Cordon control with spatially-varying metering rates: A reinforcement learning approach. Transportation Research Part C: Emerging Technologies 98, 358–369.

Ntziachristos, L., Gkatzoflias, D., Kouridis, C., Samaras, Z., 2009. COPERT: a european road transport emission inventory model. In: Information technologies in environmental engineering. Springer, pp. 491–504.

Papageorgiou, M., Diakaki, C., Dinopoulou, V., Kotsialos, A., Wang, Y., 2003. Review of road traffic control strategies. Proceedings of the IEEE 91 (12), 2043–2067.

Sirmatel, I. I., Geroliminis, N., 2017. Economic model predictive control of large-scale urban road networks via perimeter control and regional route guidance. IEEE Transactions on Intelligent Transportation Systems.

Tettamanti, T., Luspay, T., Kulcsár, B., Péni, T., Varga, I., 2014. Robust control for urban road traffic networks. IEEE Transactions on Intelligent Transportation Systems 15 (1), 385–398.

Visioli, A., 2006. Practical PID control. Springer Science & Business Media.

Wang, F.-Y., 2010. Parallel control and management for intelligent transportation systems: Concepts, architectures, and applications. IEEE Transactions on Intelligent Transportation Systems 11 (3), 630–638.

Yildirimoglu, M., Geroliminis, N., 2014. Approximating dynamic equilibrium conditions with macroscopic fundamental diagrams. Transportation Research Part B: Methodological 70, 186–200.

Yildirimoglu, M., Ramezani, M., Geroliminis, N., 2015. Equilibrium analysis and route guidance in large-scale networks with MFD dynamics. Transportation Research Part C: Emerging Technologies 59, 404–420.

Zhao, D., Dai, Y., Zhang, Z., 2012. Computational intelligence in urban traffic signal control: A survey. IEEE Transactions on Systems, Man, and Cybernetics, Part C (Applications and Reviews) 42 (4), 485–494.

Zhong, R., Chen, C., Huang, Y., Sumalee, A., Lam, W., Xu, D., 2018a. Robust perimeter control for two urban regions with macroscopic fundamental diagrams: a control-lyapunov function approach. Transportation Research Part B: Methodological 117, 687–707.

Zhong, R., Huang, Y., Chen, C., Lam, W., Xu, D., Sumalee, A., 2018b. Boundary conditions and behavior of the macroscopic fundamental diagram based network traffic dynamics: A control systems perspective. Transportation Research Part B: Methodological 111, 327–355.

Zhou, Z., De Schutter, B., Lin, S., Xi, Y., 2017. Two-level hierarchical model-based predictive control for large-scale urban traffic networks. IEEE Transactions on Control Systems Technology 25 (2), 496–508.